

A revisit of the development of viscoplastic flow in pipes and channels

Alexandros Syrakos^{a,*}, Evgenios Gryparis^{a,b}, Georgios C. Georgiou^b

^a*Department of Mechanical and Manufacturing Engineering, University of Cyprus, P.O. Box 20537, 1678 Nicosia, Cyprus*

^b*Department of Mathematics and Statistics, University of Cyprus, PO Box 20537, 1678, Nicosia, Cyprus*

Abstract

This study revisits the development of viscoplastic flow in pipes and channels, focusing on the flow of a Bingham plastic. Using finite element simulations and the Papanastasiou regularisation, results are obtained across a range of Reynolds and Bingham numbers. The novel contributions of this work include: (a) investigating a definition of the development length based on wall shear stress, a critical parameter in numerous applications; (b) considering alternative definitions of the Reynolds number in an effort to collapse the development length curves into a single master curve, independent of the Bingham number; (c) examining the patterns of yielded and unyielded regions within the flow domain; and (d) assessing the impact of the regularisation parameter on the accuracy of the results. The findings enhance the existing literature, providing a more comprehensive understanding of this classic flow problem.

Keywords: Development length, viscoplastic flow, Poiseuille flow, Bingham fluid

1. Introduction

The flow in pipes and channels is a simple yet very important case of flow. If the pipe or channel has uniform cross-section and is straight and long enough then the flow can be approximated as fully developed (Poiseuille) throughout, which greatly simplifies calculations. However, in reality, close to the entrance of the conduit or wherever there

*Corresponding author

Email addresses: syrakos.alexandros@ucy.ac.cy (Alexandros Syrakos), gryparis.evgenios@ucy.ac.cy (Evgenios Gryparis), georgiou-x.georgios@ucy.ac.cy (Georgios C. Georgiou)

is a change in cross-section, a bifurcation, a bend, or any other cause of disturbance, the flow will deviate from its fully-developed state and the fluid will have to travel some distance until it resettles. Knowledge of this development length is very desirable in many applications, for example in microfluidics [1, 2], haemodynamics [3, 4], or the petroleum industry [5].

Due to the simplicity and importance of pipe flow development, it has been studied for over a century (at least the Newtonian case); a comprehensive list of publications is provided in [6]. Unless the momentum of the flow is very small, the development length is determined by the relative strength of the viscous forces compared to inertia, with the former tending to decrease this length and the latter tending to increase it; eventually, the viscous forces harness the momentum and pin the flow to its fully developed state. Under these conditions, the development length should be proportional to the ratio of inertia to viscous forces, i.e. to the Reynolds number. Most past studies mainly focused on obtaining the constant of proportionality. Nevertheless, it was relatively recently that Durst et al. [6] pointed out that when inertia is very small the development length is actually determined by a competition between the viscous forces themselves, and hence when the Reynolds number tends to zero the development length tends to a finite, non-zero value.

Flow development is more complex when the fluid is non-Newtonian. There being different kinds of non-Newtonian behaviour, the flow development of each class of non-Newtonian fluids exhibits its own distinct characteristics. The cases of generalised Newtonian [7, 8, 9, 10] and viscoplastic flows [11, 7, 12, 13, 14] have been studied more extensively compared to the viscoelastic case [15, 16]. One complication compared to the Newtonian case is that the standard definition of the development length as the location along the centreline (or midplane) where the velocity reaches 99% of its fully developed value may no longer be an accurate indicator of the overall development of the flow. This is particularly evident in the case of viscoplastic flows, as shown in [7, 13]. The arbitrary 99% mark is set because, in the absence of a yield stress, the flow approaches its fully developed velocity asymptotically. But in viscoplastic flow an unyielded plug forms in the central region of the pipe or channel, whose velocity is everywhere fully developed

and uniform. This, in combination with the fact that viscoplasticity makes the fully developed velocity profile more blunt and hence reduces the difference in velocity between the inlet and the plug, causes the standard centreline development length to decrease as the Bingham number increases. Yet in the yielded region between the plug and the walls the flow may continue to develop for a significant distance downstream of the point where the plug starts to form. Using indicators other than the centreline development length reveals that it is in fact not true that increased viscoplasticity results in earlier development. The similarities between shear-thinning and viscoplasticity raises the suspicion that the standard development length definition may be inadequate also for shear-thinning flows, which was recently confirmed in [10].

What other indicators can be used, that give a more accurate picture? Ookawara et al. [7], who were the first to note that in Bingham flow the velocity develops faster at the centreline than elsewhere, proposed an alternative definition of the development length as the axial distance required for the velocity to reach 99% of its fully developed value at a radial location of 95% of the plug radius, a definition adopted also by Poole and Chhabra [12]. Philippou et al. [13] examined the development lengths at all radial (or spanwise) locations, and defined the “global development length” as their maximum (this length will be defined more precisely later, as it is among those that we shall use). They also examined a version of this length restricted to radial or spanwise locations where the fully developed velocity is larger than the inlet velocity. Recently, Lambride et al. [10] proposed the wall shear stress development length, which is the distance from the entrance beyond which the shear stress at the channel or pipe walls has stabilised within 1% of its fully developed value. This happens to be equivalent to the slip velocity development length in cases with Navier slip [17]. The motivation for defining this development length is twofold: on one hand, for certain flows (e.g. haemodynamics [18]) the wall shear stress is one of the most important quantities of interest; and on the other hand, shear stress is one of the major factors that govern the flow development.

An additional complication is that whereas Newtonian flow is determined by a single dimensionless number – the Reynolds number – the constitutive equations of non-Newtonian

fluids give rise to additional dimensionless numbers upon which the development length is also dependent. So, at first glance, the Newtonian convenience of having a single indicator of flow development is lost. However, some deeper consideration suggests that, if attention is restricted to generalised Newtonian and viscoplastic fluids, it may be possible to correlate the flow development to a single dimensionless parameter that has the significance of a Reynolds number; indeed, as mentioned above, provided that inertia is not very small, the flow development of such fluids is determined by the relative strength of viscous/viscoplastic forces compared to inertia, which is precisely what the Reynolds number quantifies. The challenge is to find definitions of the Reynolds number that employ general representative inertial fluxes and viscous/viscoplastic forces that govern the flow development irrespective of the particularities of each non-Newtonian constitutive model – for example, by postulating that the development length is governed by the ratio of the average momentum flux to the wall shear stress, irrespective of the kind of fluid. If such a definition is successful, it will collapse the development length curves of the various non-Newtonian flows onto the Newtonian one. The downside is that proceeding to actually calculate the values of such Reynolds numbers requires knowledge of the flow field (e.g. in order to calculate the wall shear stress in the aforementioned example). Therefore, the resulting mathematical expressions will be more complicated and will require more effort to derive compared to the standard definitions of the Reynolds number.

Efforts to find such Reynolds numbers have been reported in the literature. For power-law fluids, Poole and Ridley [8] tested three different Reynolds numbers, comparing the average momentum flux to: (a) a stress calculated from a characteristic shear rate equal to the mean velocity divided by the pipe diameter; (b) a stress calculated similarly, but using the wall viscosity instead of the characteristic shear rate viscosity; and (c) the wall shear stress. They referred to the latter as the “Metzner-Reed” Reynolds number because it was proposed by Metzner and Reed [19] in order to maintain for power-law flow the same relationship between the Reynolds number and the friction factor as for Newtonian flow. The Metzner-Reed Reynolds number proved to be the most successful in [8], and has been used also by other researchers in the past (see references in [8]). It is one of

the numbers examined in the present study, adapted for viscoplastic flow. Ookawara et al. [7] proposed Reynolds numbers for power-law and Bingham fluids, respectively, which were relatively successful in collapsing the respective development length curves onto the Newtonian one, thus providing a single curve for all three classes of fluids. The derivation of these Reynolds numbers in [7] is not entirely clear; Poole and Chhabra [12] assumed that the viscoplastic variant is the Metzner-Reed equivalent for viscoplastic flow, but this does not appear to be entirely accurate (see the present discussion in Sec. 3.3). Nevertheless, Ookawara’s viscoplastic Reynolds number was adopted in [12, 13], and both studies verified that it does a good job collapsing the development length curves onto the Newtonian one.

These approaches are based on the assumption that the development length is determined by the competition between inertia and viscous (viscoplastic) resistance, which is invalid when the Reynolds number is too small. In the low inertia regime, what governs the development length is competition between the stresses themselves, which depends on the constitutive equation and its parameters. Hence, in this regime the development length curves cannot be made to collapse no matter what definition of the Reynolds number is chosen. This was noted in [8] for power-law fluids and in [12, 13] for viscoplastic fluids whereas it seems to have been overlooked previously, when the low inertia regime was overlooked (just like for Newtonian flows).

Although beyond the scope of the present paper, it is perhaps useful to mention that it seems unlikely that such a single flow development indicator can be found for non-Newtonian flows that are governed by constitutive equations with additional time derivatives, such as viscoelastic and thixotropic flows. Such flows are also determined by other time scales (e.g. the relaxation time of viscoelastic flows) in addition to the viscous time scale embodied nondimensionally in the Reynolds number, and unless these additional time scales are sufficiently smaller than the viscous one, the Reynolds number cannot inform us of the overall time scale of flow development. For viscoelastic flows, it has been found that elasticity causes the flow to develop more slowly than a corresponding Newtonian one (e.g. [8, 20, 21, 16]) or a generalised Newtonian one that exhibits the same

degree of shear-thinning [22]. The thixotropic case has been studied relatively little, with only a few experimental [23] and computational [24] investigations available.

In the present paper we revisit the viscoplastic entrance flow problem, comparing several definitions of the Reynolds number in their ability to provide development length correlations that are independent of the degree of viscoplasticity of the flow. Different definitions of the development length are employed, including the standard (centreline), global, and wall shear stress lengths. To keep things simple, we only consider a Bingham fluid (no shear thinning or thickening). The flow is computed numerically, with a finite element method, using Papanastasiou regularisation [25] as with most previous studies. Compared to previous studies, though, we examine in detail also the pattern of yielded/unyielded zones, something that was previously missing from the literature. The effect of the regularisation parameter on the solution accuracy is also investigated. We begin with a description of the problem in Section 2, including the definitions of the various development lengths in subsection 2.2. The alternative definitions of the Reynolds number are presented in Section 3. Our results are presented in Section 4, and the paper concludes with Section 5.

2. Problem description and governing equations

Consider the isothermal flow of a Bingham fluid entering a long horizontal cylindrical tube of radius $R = D/2$, where D is the diameter, or a long horizontal infinite-width planar channel of semi-height H . The first geometry is axisymmetric, with (r, z) denoting the radial and axial coordinates, while the second is described by a Cartesian coordinate system with (x, y) denoting the directions parallel and perpendicular to the channel walls. Figure 1 shows a sketch of the axisymmetric arrangement, but the channel case is similar. At the inlet, the axial velocity is uniform, $u_z = U$, and the radial velocity is zero, $u_r = 0$. At the outlet, located sufficiently far from the inlet, the flow is assumed to be fully developed, so that $u_r = 0$ and $\partial u_z / \partial z = 0$. The no-slip condition is imposed at the wall. Along the axis (or plane) of symmetry, the standard symmetry conditions of zero radial velocity and shear stress are imposed. Due to the similarity between the axisymmetric

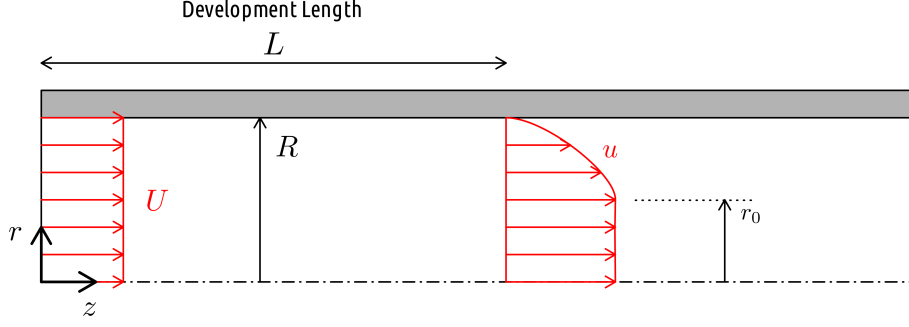


Figure 1: Development of axisymmetric viscoplastic flow in a pipe.

and planar cases, for the sake of conciseness we will describe mainly the axisymmetric case, noting any important differences between the two cases.

2.1. Governing equations

The governing equations for steady-state flow are the continuity equation,

$$\nabla \cdot \underline{u} = 0 \quad (1)$$

the momentum equation,

$$\rho \underline{u} \cdot \nabla \underline{u} = -\nabla p + \nabla \cdot \underline{\underline{\tau}} \quad (2)$$

and the Bingham constitutive equation,

$$\begin{cases} \dot{\underline{\underline{\gamma}}} = 0 & \tau \leq \tau_0 \\ \underline{\underline{\tau}} = \left(\frac{\tau_0}{\dot{\underline{\underline{\gamma}}}} + \mu \right) \dot{\underline{\underline{\gamma}}} & \tau > \tau_0 \end{cases} \quad (3)$$

where ρ is the (constant) fluid density, \underline{u} is the velocity vector, p is the pressure, $\underline{\underline{\tau}}$ is the extra stress tensor and $\tau = \sqrt{(\underline{\underline{\tau}} : \underline{\underline{\tau}})/2}$ is its magnitude, $\dot{\underline{\underline{\gamma}}} = \nabla \underline{u} + (\nabla \underline{u})^T$ is the rate-of-strain tensor and $\dot{\underline{\underline{\gamma}}}$ is its magnitude, τ_0 is the yield stress, and the constant μ is called the “plastic viscosity”. When the yield stress is zero, the Bingham constitutive equation reduces to the Newtonian one.

2.2. Development lengths

As in [13], let us define the function $L(r)$ (or $L(y)$ in planar flow) as the minimum axial distance from the entrance beyond which the velocity $u_z(r, z)$ differs from the fully

developed profile $\bar{u}_z(r)$ by no more than 1%. The standard development length concerns the velocity $u_z(0, z)$ at the centreline (midplane), and hence it is equal to $L_c = L(0)$. As mentioned in Section 1, this length may not be representative of the overall flow development, hence we can also define the global development length L_g [13] as the maximum value of $L(r)$ over all radii, $L_g = \max_{0 \leq r \leq R} L(r)$. Finally, as also mentioned in Section 1, it is useful to define also the wall shear stress development length $L_{\tau w}$, as the minimum length beyond which the shear stress at the wall remains within a $\pm 1\%$ margin of its fully-developed value.

2.3. Dimensionless equations and numbers

Scaling lengths by the pipe radius R or the channel semi-height H , velocities by the inlet velocity U , and the pressure and stress by $\mu U/R$ (or $\mu U/H$), the continuity, momentum, and constitutive equations are converted to the following non-dimensional forms, respectively:

$$\tilde{\nabla} \cdot \tilde{\underline{u}} = 0 \quad (4)$$

$$\frac{1}{2} Re \tilde{\underline{u}} \cdot \tilde{\nabla} \tilde{\underline{u}} = -\tilde{\nabla} \tilde{p} + \tilde{\nabla} \cdot \tilde{\underline{\tau}} \quad (5)$$

$$\begin{cases} \tilde{\underline{\gamma}} = 0 & \tilde{\tau} \leq Bn/2 \\ \tilde{\underline{\tau}} = \left(\frac{Bn}{2\tilde{\gamma}} + 1 \right) \dot{\underline{\gamma}} & \tilde{\tau} > Bn/2 \end{cases} \quad (6)$$

The dimensionless numbers appearing in the above equations are the standard Reynolds number,

$$Re \equiv \frac{2\rho UR}{\mu} \quad (7)$$

and the Bingham number,

$$Bn \equiv \frac{2\tau_0 R}{\mu U} \quad (8)$$

(with R replaced by H in the planar case). To be consistent with the rest of the literature, these numbers are based on the pipe diameter $2R$ or channel height $2H$, hence the $1/2$

factors appearing in the governing equations. The dimensionless yield stress is equal to $\tilde{\tau}_0 = Bn/2$.

2.4. Fully developed flow

A brief description of the fully developed (Poiseuille) flow will facilitate the discussion in the subsequent sections. Let us denote the pressure gradient by $G = -dp/dz$. In fully developed flow, the pressure gradient is balanced by the shear stress, whose magnitude is zero at the centre and increases linearly towards the walls:

$$\tau_{rz} = \frac{1}{2}Gr \quad (9)$$

This means that for any finite value of yield stress, $\tau_0 > 0$, there will be an unyielded cylindrical plug at the centre of the pipe with radius

$$r_0 = \frac{2\tau_0}{G} \quad (10)$$

Note that there will be no flow if $r_0 \geq R$. The fully developed velocity profile is:

$$\bar{u}_z(r) = \frac{G}{4\mu} \begin{cases} (R - r_0)^2, & 0 \leq r \leq r_0 \\ [(R - r_0)^2 - (r - r_0)^2], & r_0 \leq r \leq R \end{cases} \quad (11)$$

and the mean velocity is related to the pressure gradient by:

$$U = G \frac{R^2}{24\mu} (3 - 4\tilde{r}_0 + \tilde{r}_0^4) \quad (12)$$

where $\tilde{r}_0 = r_0/R$ is the non-dimensional plug radius, which is a convenient indicator of the viscoplasticity of the flow, alternative to the Bingham number. Their relationship can be found by substituting τ_0 from (10) and U from (12) into the Bingham number definition (8):

$$Bn = \frac{24\tilde{r}_0}{3 - 4\tilde{r}_0 + \tilde{r}_0^4} \quad (13)$$

This is a one-to-one relationship between them, so they convey the same information.

A useful expression for the wall shear stress τ_w is obtained by setting $r = R$ in Eq. (9) and using Eq. (12) to substitute for the pressure gradient:

$$\tau_w = \frac{12\mu U}{R} \frac{1}{3 - 4\tilde{r}_0 + \tilde{r}_0^4} \quad (14)$$

2.4.1. Planar flow

In planar Poiseuille Bingham flow, Eqs. (9) – (14) are replaced by:

$$\tau_{yx} = Gy \quad (15)$$

$$y_0 = \frac{\tau_0}{G} \quad (16)$$

$$\bar{u}_x(y) = \frac{G}{2\mu} \begin{cases} (H - y_0)^2, & 0 \leq y \leq y_0 \\ [(H - y_0)^2 - (y - y_0)^2], & y_0 \leq y \leq H \end{cases} \quad (17)$$

$$U = G \frac{H^2}{6\mu} (2 - 3\tilde{y}_0 + \tilde{y}_0^3) \quad (18)$$

$$Bn = \frac{12\tilde{y}_0}{2 - 3\tilde{y}_0 + \tilde{y}_0^3} \quad (19)$$

$$\tau_w = \frac{6\mu U}{H} \frac{1}{2 - 3\tilde{y}_0 + \tilde{y}_0^3} \quad (20)$$

where $\tilde{y}_0 = y_0/H$ is the dimensionless half-thickness of the plug.

2.5. Solution method

The equations were solved in dimensionless form. For the numerical solution, the constitutive equation (6) was regularised according to the popular method of Papanastasiou [25]:

$$\underline{\underline{\tilde{\tau}}} = \left[\frac{Bn (1 - e^{-M\tilde{\gamma}})}{2\tilde{\gamma}} + 1 \right] \underline{\underline{\tilde{\gamma}}} \quad (21)$$

where $M = mU/R$, m being the dimensional regularisation parameter. This method has been used also in previous studies [12, 13] in order to avoid the difficulties associated with the discontinuous nature of the original Bingham equation. The introduced parameter M must have a sufficiently large value in order for Eq. (21) to mimick the original equation (6) accurately. Values of $M \geq 500$ are generally considered adequate [25, 26, 12, 27, 28] for most purposes, unless one wants to capture the yield surfaces with high accuracy. However, for the present flow we will see later that higher values of M may be required at higher Reynolds numbers.

The governing equations were solved with a standard Galerkin finite element method employing biquadratic and bilinear basis functions for the velocity and pressure, respectively. The simulations were performed using the open-source finite element package FEniCS [29] (fenicsproject.org); in selected cases the results were validated against predictions by an in-house code [13]. There was no noticeable difference between the predictions of the two codes.

3. Alternative Reynolds numbers

3.1. The effective Reynolds number

Recognising that in viscoplastic flows it is more illuminating to compare inertia to a characteristic *viscoplastic* force rather than to its viscous component only, various authors have replaced the plastic viscosity μ in Eq. (7) with an effective viscosity of $\mu_{\text{eff}} = \tau_0/\dot{\gamma}_c + \mu$, where $\dot{\gamma}_c$ is a characteristic strain rate of the flow. The resulting Reynolds number is referred to as “effective” or “modified” Reynolds number,

$$Re^* = \frac{\rho U^2}{\tau_0 + \mu \dot{\gamma}_c} \quad (22)$$

and has been shown to be much more useful as a flow regime indicator than the standard Reynolds number [30, 31, 32, 33]; it conveys information about the flow even on its own, whereas the standard Reynolds number tells us nothing about the flow unless it is accompanied by the Bingham number. Thompson and Soares [32] strongly advocate for the adoption of this Reynolds number, even proposing that the definition (22) should be

referred to simply as the “Reynolds number” without further qualification. The reasoning is that the definition (22) conveys analogous information for viscoplastic flows as the standard Reynolds number does for Newtonian flows, quantifying the ratio between inertia and the internal forces that resist the development of velocity gradients.

The “effectiveness” of the effective Reynolds number depends on the selection of a truly characteristic rate of strain $\dot{\gamma}_c$, which is art as much as it is science. The choice $\dot{\gamma}_c = U/D$ affords the analogue of the “Collins-Schowalter” Reynolds number for power-law flow [8]:

$$Re^{*D} = \frac{\rho U^2}{\tau_0 + \mu U/D} = \frac{Re}{Bn+1} = Re \frac{3 - 4\tilde{r}_0 + \tilde{r}_0^4}{3 + 20\tilde{r}_0 + \tilde{r}_0^4} \quad (23)$$

However, intuitively, it seems that U/D rather under-represents the shear rates occurring in the pipe, whereas U/R seems more typical of a mean shear rate between the wall (where the velocity is zero) and the centre of the pipe (where the velocity is actually greater than U). Therefore, in order to investigate the effect of the choice of $\dot{\gamma}_c$, we define also the effective Reynolds number based on the radius:

$$Re^{*R} = 2 \frac{\rho U^2}{\tau_0 + \mu U/R} = 2 \frac{Re}{Bn+2} \quad (24)$$

where the factor 2 has been introduced so that for Newtonian flow ($Bn = 0$) Re^{*R} and Re become identical.

Planar case

In the planar case, the respective Reynolds numbers are given by the same formulae as for the axisymmetric one:

$$Re^{*2H} = \frac{Re}{Bn+1} \quad , \quad Re^{*H} = 2 \frac{Re}{Bn+2} \quad (25)$$

3.2. The Metzner-Reed Reynolds number

Arguably, the fully developed wall shear stress τ_w is much more crucial for driving the dynamics of this flow than a shear stress based on $\dot{\gamma}_c = U/D$ or even $\dot{\gamma}_c = U/R$. So, let

us replace the latter with the former in (23) to define the following Reynolds number:

$$Re_{MR} = 8 \frac{\rho U^2}{\tau_w} \quad (26)$$

The factor 8 has been introduced so that Re_{MR} reduces to Re when the flow is Newtonian. Using Eq. (14), Re_{MR} can be expressed as:

$$Re_{MR} = Re \frac{3 - 4\tilde{r}_0 + \tilde{r}_0^4}{3} \quad (27)$$

We will call Re_{MR} the ‘‘Metzner-Reed’’ Reynolds number because the reasoning behind it is essentially the same as for the analogous Reynolds number that Metzner and Reed [19] proposed for power-law fluids. Metzner and Reed designed their Reynolds number so that, for power-law fluids, it would relate to the friction factor in the same way that the standard Reynolds number relates to it in laminar Newtonian flows: $Re = 16/f$, where $f = \tau_w/(\frac{1}{2}\rho U^2)$ is the Fanning friction factor [19].

Note that, just like the relationship $Re = 16/f$ does not hold for turbulent Newtonian flow, the expressions (26) and (27) are no longer equivalent for turbulent Bingham flow for which the wall shear stress is not given by Eq. (14) (the present study is limited to laminar flows). Expression (26) is more general, applying across different fluid types and flow regimes. In fact, it has been used for viscoplastic pipe flow by Kfuri et al. [5]. Re_{MR} can be straightforwardly calculated from measurements, since the average velocity U is readily obtained from the flow rate Q as $U = Q/A$, where A is the pipe’s cross-sectional area, and the wall shear stress can be obtained from the pressure gradient G from Eq. (9) at $r = R$. If the pipe is not circular, then the corresponding expression is $\tau_w = G(A/S)$ where S is the periphery of the pipe’s cross-section; for arbitrary cross-sectional shapes, this would return an average value of τ_w around the wall.

Planar case

In the planar case, instead of (27) we obtain:

$$Re_{MR} = Re \frac{2 - 3\tilde{y}_0 + \tilde{y}_0^3}{2} \quad (28)$$

3.3. Applying a momentum correction

As mentioned in Section 1, it was Ookawara et al. [7] who first proposed a Reynolds number definition for the development of Bingham flow in a pipe that results in a correlation that is close to that for Newtonian flow. Their definition was later used by other authors as well [12, 13]. Ookawara et al. did not provide a detailed derivation of their Reynolds number, but it appears to be based on Eq. (26) with a correction factor applied to the momentum flux in the numerator. Let us follow such an approach, and define a “momentum-corrected” version of Eq. (26) as:

$$Re_{MRC} = \alpha \frac{\frac{1}{A} \int_A \rho \bar{u}^2 dA}{\tau_w} \quad (29)$$

We have therefore replaced the numerator ρU^2 of Eq. (26) by the more accurate momentum flux $(1/A) \int_A \rho \bar{u}^2 dA$ where A denotes the pipe cross-section or its area, and $\bar{u}(r)$ is the fully-developed velocity. The number α in the expression is a scaling factor, playing the same role as “8” in Eq. (26) in ensuring that the Reynolds number (29) reduces to the standard one (Eq. (7)) in Newtonian flow.

Re_{MRC} requires more detailed knowledge about the flow compared to the previous Reynolds numbers; in particular, it requires knowledge of the fully-developed velocity profile. In the present case the velocity profile is given by Eq. (11). Integrating, and using $\tau_w = GR/2$ and Eq. (12) one arrives at:

$$Re_{MRC} = Re \frac{3}{5} \frac{(1 - \tilde{r}_0)^2 (5 + 6\tilde{r}_0 + 4\tilde{r}_0^2)}{3 + 2\tilde{r}_0 + \tilde{r}_0^2} \quad (30)$$

where the expression has been scaled so that $Re_{MRC} = Re$ for $\tilde{r}_0 = 0$.

The above expression can be manipulated into an alternative form by substituting for $(1 - \tilde{r}_0)^2$ using the identity

$$(3 + 2\tilde{r}_0 + \tilde{r}_0^2) (1 - \tilde{r}_0)^2 = 3 - 4\tilde{r}_0 + \tilde{r}_0^4 \quad (31)$$

to arrive at

$$Re_{MRC} = Re \frac{1}{3} \left(3 - 4\tilde{r}_0 + \tilde{r}_0^4 \right) \frac{9}{5} \frac{5 + 6\tilde{r}_0 + 4\tilde{r}_0^2}{(3 + 2\tilde{r}_0 + \tilde{r}_0^2)^2} \quad (32)$$

Expression (32) is almost identical with the expression proposed by Ookawara et al. [7], but there is one difference: in [7], the last term in the numerator is $-11\tilde{r}_0^2$ instead of the $4\tilde{r}_0^2$ of Eq. (32). Given that the whole of the numerator of the fraction appearing at the end of expression (32) comes from the integration of the velocity profile, it is difficult to see how any modification to the assumptions or rationale behind Re_{MRC} could bring about a change in a single coefficient. We did not pursue further efforts to derive the formula of [7].

It may be useful for purposes of generalisability to discuss another path to arrive at expression (30). Consider a length l of the pipe where the flow is fully developed; the kinetic energy of the fluid contained in this length of pipe is:

$$E = \int_A \frac{1}{2} \rho l \bar{u}^2 dA \quad (33)$$

This kinetic energy is constantly being dissipated by viscous stresses, but at the same time replenished by the work of pressure so that it remains constant. The rate of work done by pressure on the volume of fluid contained in the length l of pipe is equal to the pressure times the velocity at the inlet minus the pressure times the velocity at the outlet. The velocity is the same at the inlet and outlet, while the pressure difference across the length l is Gl . Therefore, the rate of work is:

$$P = \int_A Gl \bar{u} dA = Gl \int_A \bar{u} dA = GlUA \quad (34)$$

As said, this is also the rate of work done by the viscous forces. The ratio E/P is the amount of time that the viscous forces would need in order to dissipate all of the fluid's kinetic energy; during that time, the fluid travels a distance $(E/P)U$, which can be considered to be proportional to the development length – it is a length scale characteristic of flow changes governed by a competition between inertia and viscosity. This would make the dimensionless development length, L/D , proportional to EU/PD which, from Eqs.

(33), (34), and $G = 2\tau_w/R$, is equal to expression (29).

Planar case

The corresponding expression in the planar case is:

$$Re_{MRC} = Re \frac{1}{4} \frac{(1 - \tilde{y}_0)^2(8 + 7\tilde{y}_0)}{2 + \tilde{y}_0} \quad (35)$$

3.4. “Momentum gain” Reynolds number

Re_{MRC} can be viewed as a dimensionless length scale for changes to occur in the flow. An idea for further enhancement may be to account also for the amount of change that occurs in each flow. For example, a viscoplastic flow with its blunt velocity profile undergoes less overall development than a Newtonian flow. We can account for this by replacing the fully developed momentum flux in the numerator of the Reynolds number by the difference between that flux and the momentum flux at the inlet:

$$Re_{MG} = \alpha \frac{\frac{1}{A} \int_A \rho \bar{u}^2 dA - \rho U^2}{\tau_w} \quad (36)$$

Comparing with Eqs. (26) and (29) we can see that Re_{MG} is a weighted combination of Re_{MR} and Re_{MRC} . Because $U = \frac{1}{A} \int_A \bar{u} dA$, the Cauchy-Schwarz inequality guarantees that the numerator of (36) is non-negative (it is zero only if $\bar{u} = U$ everywhere).

For our particular flow, integrating (11), using $\tau_w = GR/2$ and Eq. (12), and scaling, we arrive at the following expression:

$$Re_{MG} = Re \frac{1}{5} (1 - \tilde{r}_0)^3 \frac{15 + 27\tilde{r}_0 + 25\tilde{r}_0^2 + 5\tilde{r}_0^3}{3 + 2\tilde{r}_0 + \tilde{r}_0^2} \quad (37)$$

Again, it may be somewhat more illuminating and conducive to the generalisability of this Reynolds number to consider an alternative path to its derivation. Let L_a be the length travelled by the fluid until the pressure gradient can accelerate it from the flat U profile to the fully developed $\bar{u}(r)$ profile, neglecting the viscous resistance. Omitting the viscous forces, the momentum balance on the volume of fluid from the inlet to a distance

L_a is (using the Reynolds transport theorem):

$$\int_A \rho \bar{u}^2 dA - \rho U^2 A = G L_a A \quad (38)$$

where we have approximated the pressure difference between the inlet and $z = L_a$ by GL_a . We can then rearrange Eq. (38) into an expression for the dimensionless length L_a/D , which, using $G = 2\tau_w/R$, is the same as (36). So, the hypothesis for a successful Re_{MG} is that the development length is proportional to L_a .

Planar case

In planar flow, instead of Eq. (37) we arrive at:

$$Re_{MG} = Re \frac{1}{2} (1 - \tilde{y}_0)^3 \frac{4 + 5\tilde{y}_0}{2 + \tilde{y}_0} \quad (39)$$

3.5. “Energy gain” Reynolds number

Finally, we could not resist the temptation to, instead of considering the pressure force and the gain in momentum, consider the pressure work and the gain in kinetic energy. This leads to the following equation, instead of Eq. (38):

$$\int_A \frac{1}{2} \rho \bar{u}^3 dA - \frac{1}{2} \rho U^3 A = \int_A G L_a \bar{u} dA = G L_a U A \quad (40)$$

which, for our flow, gives rise to the following Reynolds number:

$$Re_{EG} = Re \frac{1}{105} (1 - \tilde{r}_0)^3 \frac{945 + 2187\tilde{r}_0 + 2520\tilde{r}_0^2 + 980\tilde{r}_0^3 + 245\tilde{r}_0^4 + 35\tilde{r}_0^5}{(3 + 2\tilde{r}_0 + \tilde{r}_0^2)^2} \quad (41)$$

Planar case

The corresponding expression for planar flow is:

$$Re_{EG} = Re \frac{1}{38} (1 - \tilde{y}_0)^3 \frac{152 + 245\tilde{y}_0 + 35\tilde{y}_0^2}{(2 + \tilde{y}_0)^2} \quad (42)$$

4. Results

Most of the results to be presented were obtained on a single graded structured mesh with a length of 300 diameters (600 radii), consisting of 206000 triangular elements. The mesh was more refined near the entrance and close to the wall, with the smallest element being a right-angled triangle of sides $\Delta r = 0.005R$ and $\Delta z = 0.01R$ at the entrance corner. The same mesh was used for both the axisymmetric and planar calculations. To ensure that the mesh length suffices even for the higher Reynolds number cases, we repeated the calculations for selected high- Re cases on a longer mesh of length $500D$ ($1000R$), but the discrepancy in the solutions was found to not be significant. A shorter, very fine, graded mesh length $20D$ ($40R$), consisting of 160000 elements was employed for a set of creeping flow ($Re = 0$) calculations where the Bingham number was varied in the range $Bn \in [0, 50]$ (to be discussed towards the end of this section). The smallest element (at the entrance corner) had sides $\Delta r = 0.001R$ and $\Delta z = 0.002R$.

Before proceeding to the comparison of the correlations of the development lengths with the various proposed Reynolds numbers, it is useful to start with a general description of the flow field, and in particular of the pattern of yielded and unyielded regions. Although, as discussed in Section 1, there already exist quite a few studies on viscoplastic flow development, a detailed description of the yield state seems to be lacking. Figure 2 shows the regions close to the entrance for pipe (Fig. 2a) and channel (Fig. 2b) flow at $Bn = 5$ and $Re = 0$, calculated with $M = 10000$. Unyielded zones are drawn in dark blue, and their boundaries (yield surfaces) are delineated in white. The apparent roughness of the yield lines (the $\tilde{\tau} = \tilde{\tau}_0 = Bn/2$ contours) is an artefact of the high value of the regularisation parameter; a lower value produces smoother contours, but at a cost of a loss of accuracy, as will be discussed later. Smooth yield lines are difficult to capture also with methods other than Papanastasiou regularisation, and a common workaround is to plot instead contours of $\tilde{\tau} = (1 + \epsilon)\tilde{\tau}_0$, where ϵ is a very small number (e.g. [34, 33]), which are usually notably smoother. However, in the present work no such margin is used ($\epsilon = 0$).

The plots of Fig. 2 also include some streamlines. Close to the entrance, the streamlines

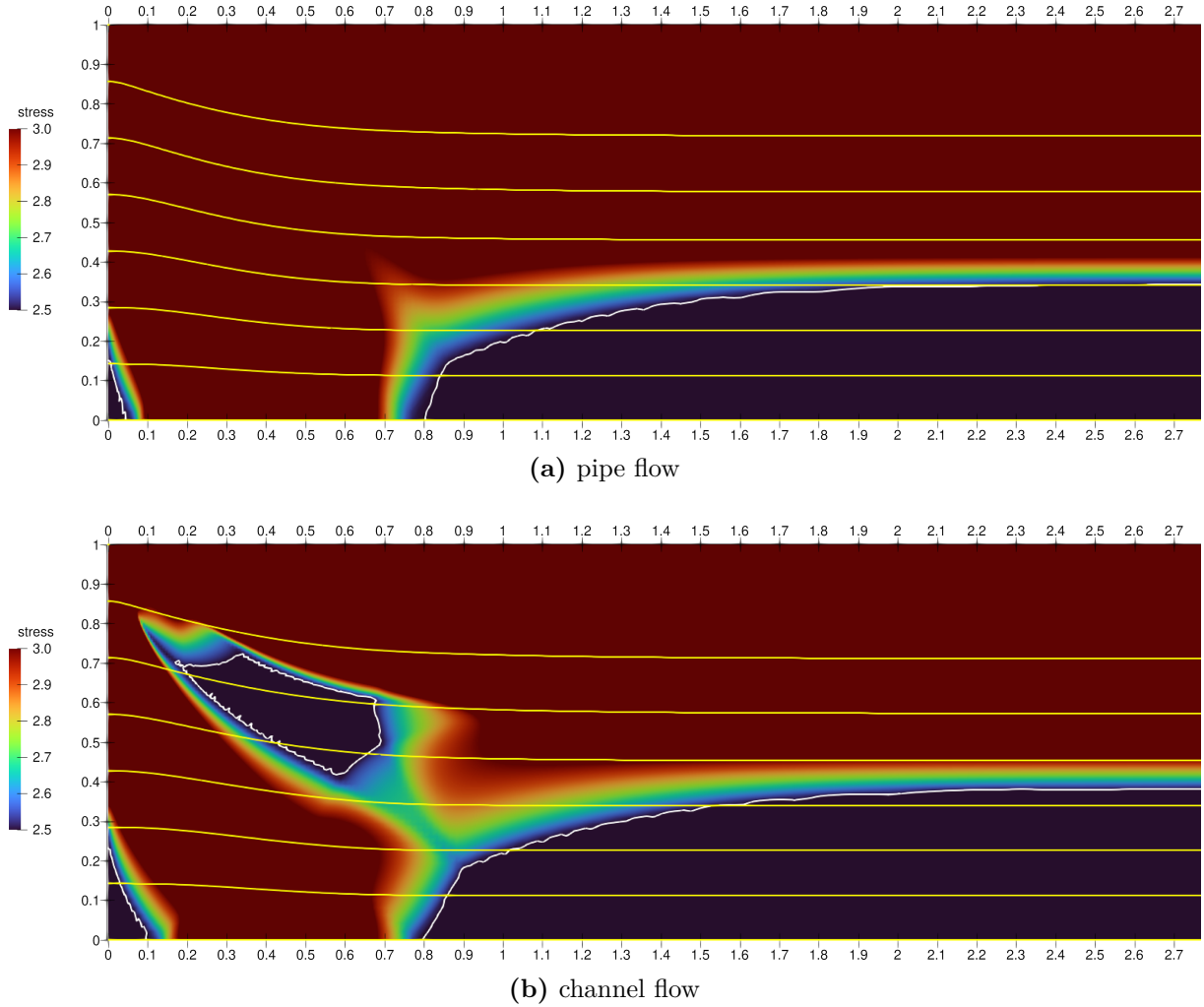


Figure 2: Contours of dimensionless stress magnitude for (a) pipe and (b) channel flow at $Bn = 5$ and $Re = 0$, calculated with $M = 10000$. The dimensionless yield stress for this case is $\tilde{\tau}_0 = Bn/2 = 2.5$, and the yield lines are drawn in white. Unyielded material ($\tilde{\tau} < 2.5$) is shown in uniform dark blue, and regions of $\tilde{\tau} > 3$ are shown in uniform dark red. Superimposed are streamlines, drawn in yellow.

are sloped away from the walls, where the flow decelerates due to the no-slip condition, and towards the centre of the pipe or channel, where the flow accelerates to compensate and satisfy continuity. The yielded/unyielded fluid patterns look qualitatively quite similar for the axisymmetric and planar cases, with one notable difference: while the former has two plug regions, the latter exhibits three. Streamlines cross the boundaries of all of these unyielded zones. As these are steady-state results, the location and size of the unyielded zones do not vary with time, yet the material contained in them moves as a solid body. This may seem perplexing at first glance, but what is actually taking place is that yielded material flows into these zones through their boundaries (where streamlines cross into them) and upon entry it solidifies due to the lowering of the stress levels. Thenceforth, all

| Bn | \tilde{r}_0 | \tilde{y}_0 |
|------|---------------|---------------|
| 0 | 0.00000 | 0.00000 |
| 1 | 0.10715 | 0.13349 |
| 2 | 0.18758 | 0.22346 |
| 5 | 0.34247 | 0.38058 |
| 10 | 0.47683 | 0.50727 |
| 20 | 0.60222 | 0.62259 |

Table 1: Dimensionless plug radii \tilde{r}_0 and thicknesses \tilde{y}_0 at various values of the Bingham number, calculated from Eqs. (13) and (19).

fluid particles in the zone move together as a rigid solid; but upon reaching the boundaries where streamlines cross out of the zone, stress levels increase, and the material liquefies again. Thus, there is a constant influx and outflux of material through the boundaries of the unyielded plugs, with the state of the material switching between yielded and unyielded upon traversing these boundaries, as discussed also, for example, in [27, 35].

In pipe flow (Fig. 2a), the unyielded zones comprise of a a small cone right at the central region of the inlet and a large cylindrical core at the centre of the pipe that begins at approximately $z/R \approx 0.8$ and grows downstream, eventually reaching the fully-developed radius $\tilde{r}_0 \approx 0.3425$ (Table 1). In the channel case (Fig. 2b) the picture looks similar, but one has to keep in mind that the three-dimensional geometry of the plugs is entirely different. Instead of a conical zone at the inlet there is a wedge, and instead of a cylindrical core there is a slab extending infinitely in the direction perpendicular to the page; the latter also begins at $x/H \approx 0.8$ and its semi-height grows to the fully-developed value $\tilde{y}_0 \approx 0.38$ (Table 1).

In the channel flow there is an additional plug zone with no analogue in the axisymmetric case: it is an oblong slanted zone near the top-left corner. This zone is also apparent in the results of Dimakopoulos et al. [34]. As seen from the curvature of the streamlines inside this zone, its motion involves solid-body rotation. Its existence seems explicable by the fact that, since the flow decelerates near the wall and accelerates near the centre, there must be an intermediate region where the velocity does not change much, and where therefore stresses remain low, giving rise to this zone. On the other hand, in the axisymmetric case the slanting of the streamlines in that region makes it impossible

for such a zone to exist. Had such a zone existed, it would actually be an annulus of unyielded material. If we then consider a ring of particles inside this zone all at the same initial radial coordinate r_A , then as they move along their streamlines their radial distance from the centreline must decrease since the streamlines are slanted inwards (towards the centreline). This means that at a later time, while still inside the zone, the same ring of particles will have a smaller radius $r_B < r_A$. But if the state of the material is that of a rigid solid, then it is impossible for a ring of such material to deform so as to reduce its radius. Hence the inwards slanting of the streamlines in that region precludes the possibility of existence of such an unyielded zone in the axisymmetric case.

The accuracy of the calculation of the yield lines can be quite sensitive to the regularisation parameter M [36, 37]. Figures 3 and 4 compare the yield lines and stress contours computed with $M = 500$ and $M = 10000$ for the creeping flow ($Re = 0$) axisymmetric and planar flows with $Bn = 5$. There are no noticeable differences, and adequate accuracy is already provided by $M = 500$. However, the situation changes if the Reynolds number is increased. Figures 5 and 6 make the same comparison, for pipe and channel flow, respectively, at a higher Reynolds number of 61 while Bn is kept at 5. While again the differences are marginal in the planar case (Fig. 6), in the axisymmetric case there is a very significant discrepancy between the results obtained with $M = 500$ (Fig. 5a) and those obtained with $M = 10000$ (Fig. 5b). The $M = 500$ results predict a significantly faster evolution of stress along the axial direction in a region upstream of the core plug, and a significantly earlier formation of the core plug by almost two pipe radii. The discrepancy becomes more pronounced with further increase of Re . Figures 7 and 8 are for $Re = 246$. Now $M = 500$ is inadequate even for the planar case. For the axisymmetric case, $M = 500$ predicts the core plug formation nearly 11.5 pipe radii upstream from where $M = 10000$ predicts it.

These results are in line with past experience according to which small values of M suffice when the yield lines are located in regions of rapid variations of stress but high values of M are required when the stress varies gradually. For example, for the lid-driven cavity benchmark problem where the flow occurs in a confined space, the unyielded regions

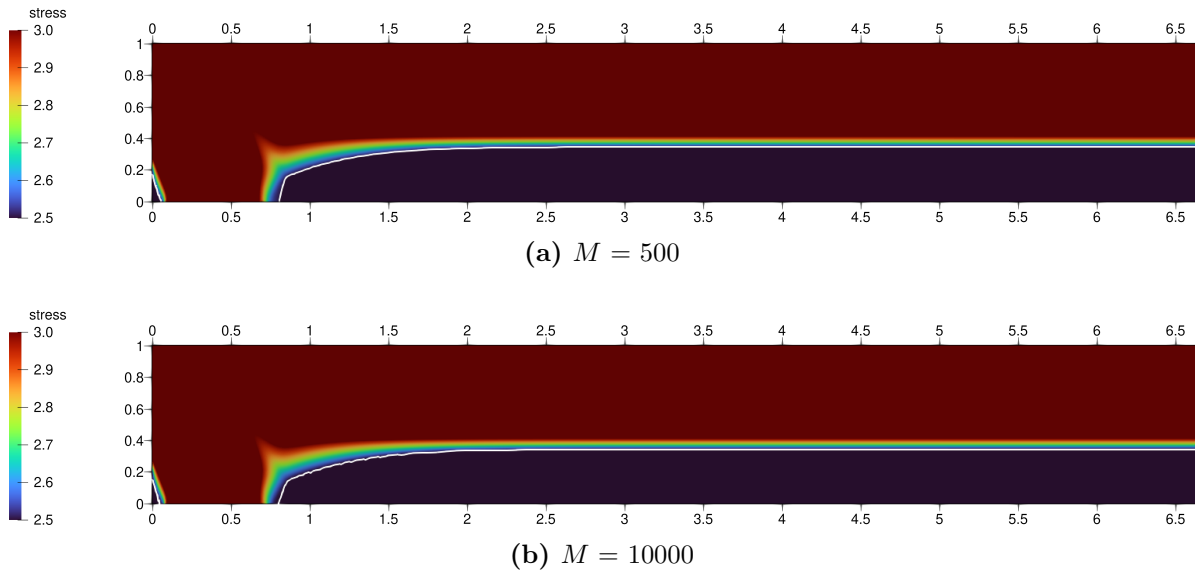


Figure 3: Pipe flow, $Bn = 5$, $Re = 0$: Contours of dimensionless stress magnitude, calculated with (a) $M = 500$ and (b) $M = 10000$. Yield lines ($\tilde{\tau} = \tilde{\tau}_0 = Bn/2 = 2.5$) are drawn in white. Unyielded material ($\tilde{\tau} < 2.5$) is shown in uniform dark blue, and regions of $\tilde{\tau} > 3$ are shown in uniform dark red.

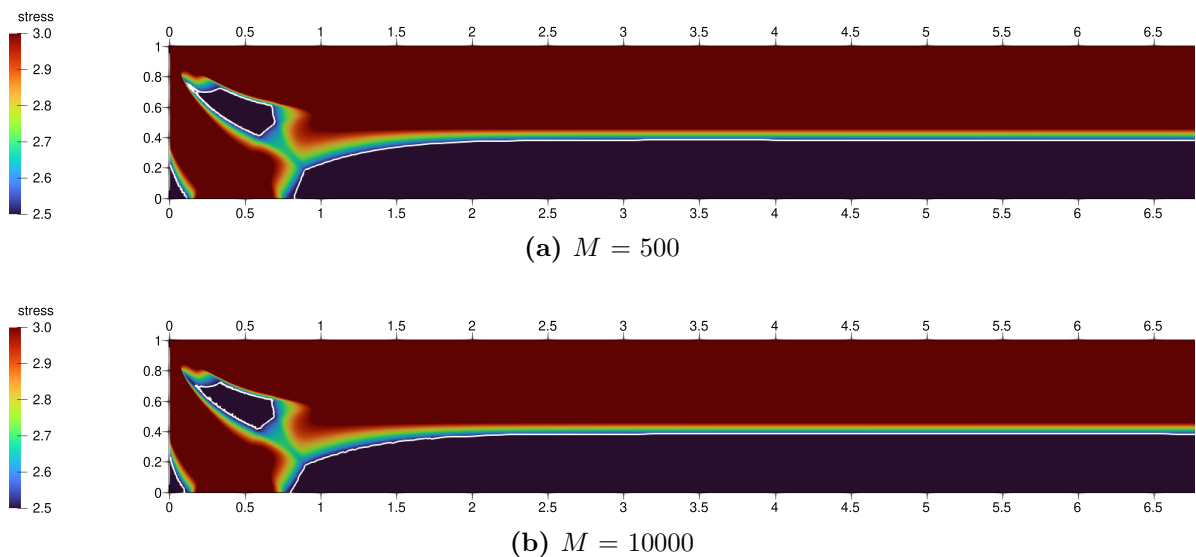


Figure 4: Channel flow, $Bn = 5$, $Re = 0$: Contours of dimensionless stress magnitude, calculated with (a) $M = 500$ and (b) $M = 10000$. Yield lines ($\tilde{\tau} = \tilde{\tau}_0 = Bn/2 = 2.5$) are drawn in white. Unyielded material ($\tilde{\tau} < 2.5$) is shown in uniform dark blue, and regions of $\tilde{\tau} > 3$ are shown in uniform dark red.

can be calculated with satisfactory accuracy using small values of M , e.g. $M = 400$ [27, 28]. For unconfined flow over a cylinder [36] low values of M can predict satisfactorily the unyielded regions that arise close to the cylinder, where the stresses exhibit large spatial gradients, but can be completely off the mark in predicting the outer extent of the yield zone caused by the presence of the cylinder, as the stresses die out very gradually in the far field. Similar observations have been made also for the rising bubble problem [37]. The

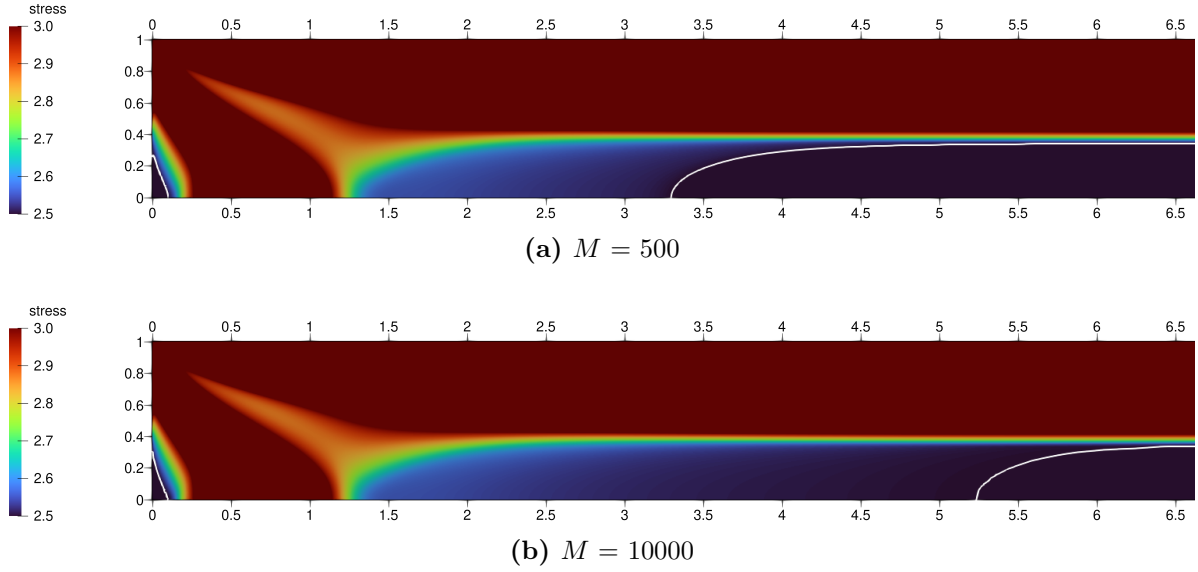


Figure 5: Pipe flow, $Bn = 5$, $Re = 61$: Contours of dimensionless stress magnitude, calculated with (a) $M = 500$ and (b) $M = 10000$. Yield lines ($\tilde{\tau} = \tilde{\tau}_0 = Bn/2 = 2.5$) are drawn in white. Unyielded material ($\tilde{\tau} < 2.5$) is shown in uniform dark blue, and regions of $\tilde{\tau} > 3$ are shown in uniform dark red.

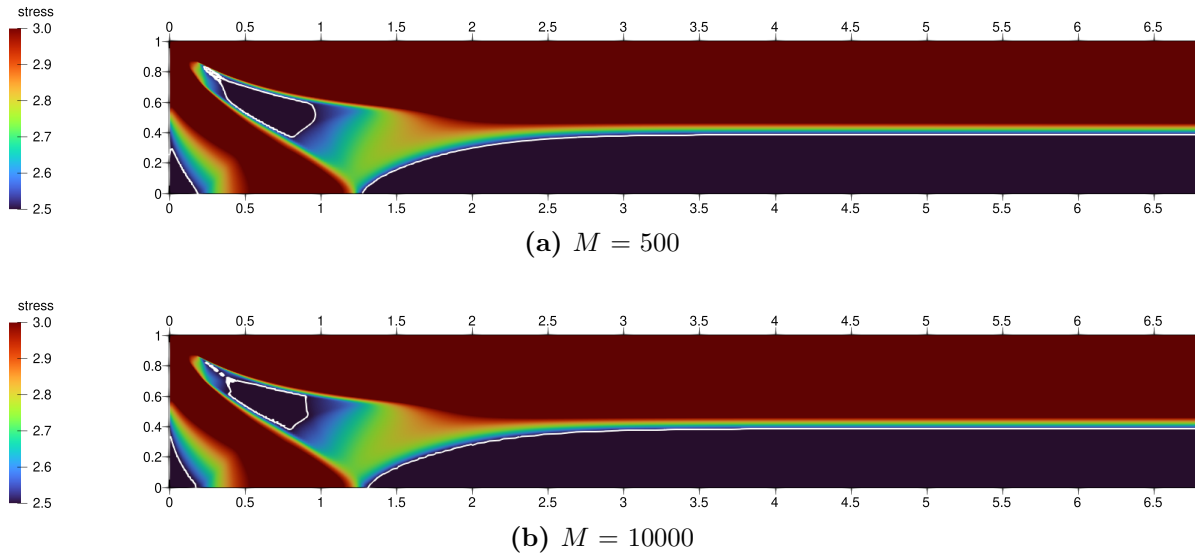
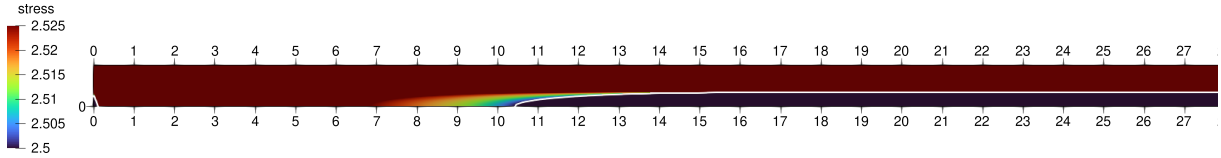
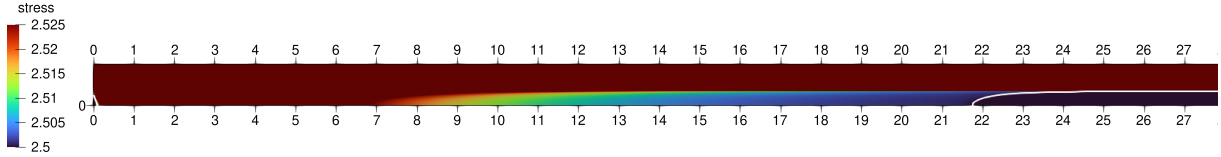


Figure 6: Channel flow, $Bn = 5$, $Re = 61$: Contours of dimensionless stress magnitude, calculated with (a) $M = 500$ and (b) $M = 10000$. Yield lines ($\tilde{\tau} = \tilde{\tau}_0 = Bn/2 = 2.5$) are drawn in white. Unyielded material ($\tilde{\tau} < 2.5$) is shown in uniform dark blue, and regions of $\tilde{\tau} > 3$ are shown in uniform dark red.

present results exhibit the same pattern. At low Reynolds numbers the flow development, determined by a competition among viscoplastic stresses themselves, occurs within a short distance from the inlet; the flow field varies rapidly, and $M = 500$ is entirely adequate to provide a good estimate of the yield lines. However, at higher Reynolds numbers the stresses are not strong enough to rein in the momentum of the incoming fluid quickly, and the flow development is gradual. These are not favourable conditions for regularisation

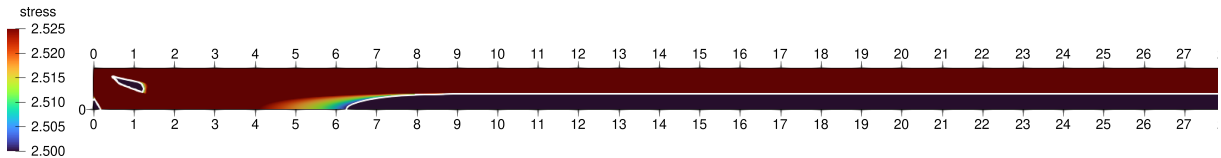


(a) $M = 500$

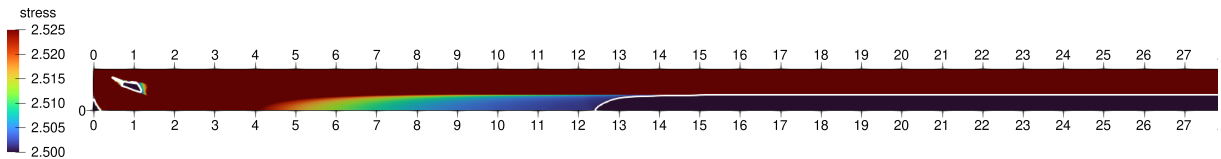


(b) $M = 10000$

Figure 7: Pipe flow, $Bn = 5$, $Re = 246$: Contours of dimensionless stress magnitude, calculated with (a) $M = 500$ and (b) $M = 10000$. Yield lines ($\tilde{\tau} = \tilde{\tau}_0 = Bn/2 = 2.5$) are drawn in white. Unyielded material ($\tilde{\tau} < \tilde{\tau}_0 = 2.5$) is shown in uniform dark blue, and regions of $\tilde{\tau} > 1.01\tilde{\tau}_0 = 2.525$ are shown in uniform dark red.



(a) $M = 500$



(b) $M = 10000$

Figure 8: Channel flow, $Bn = 5$, $Re = 246$: Contours of dimensionless stress magnitude, calculated with (a) $M = 500$ and (b) $M = 10000$. Yield lines ($\tilde{\tau} = \tilde{\tau}_0 = Bn/2 = 2.5$) are drawn in white. Unyielded material ($\tilde{\tau} < \tilde{\tau}_0 = 2.5$) is shown in uniform dark blue, and regions of $\tilde{\tau} > 1.01\tilde{\tau}_0 = 2.525$ are shown in uniform dark red.

to capture the yield lines and thus we see that high values of M are required. In Fig. 7b the colour contours indicate that the stress magnitude upstream of the unyielded core varies by only 1% over a length of 15 pipe radii, something that can be captured with $M = 10000$ but not with $M = 500$.

These results may raise concern about the ability of regularisation methods to accurately compute the development length. However, typically other flow features (e.g. the velocity and pressure fields) are much more accurately predicted compared to the yield lines. This turns out to be true in the present case as well. Figure 9 shows the variation of the local development length $L(r)$ or $L(y)$ across the pipe radius or channel width, as

computed for various values of M , for $Bn = 5$ and $Re = 0, 61,$ and 246 . The blue lines depict the development length beyond which the velocity remains within 1% of its fully developed value, but also included are the red lines which mark the development length for settling within 0.5% of the fully developed velocity. Let us denote these lengths as $L_{1\%}$ and $L_{0.5\%}$, respectively. In the axisymmetric case (left column of diagrams) it may be seen that even $M = 500$ can be considered adequate for accurate calculation of $L_{1\%}$ in all three cases shown, which may come as a surprise given the discrepancy between figures 7a and 7b. The calculation of $L_{0.5\%}$ is more demanding, with $M = 2000$ being a better choice that ensures accuracy. Interestingly, the planar case seems to require higher values of M , of the order of 2000, or even 5000 for $Re = 246$, to accurately capture $L_{1\%}$ close to the wall. The situation is worse for $L_{0.5\%}$, for which values of M in excess of 10000 are required in the $Re = 246$ case in order to achieve accuracy close to the wall.

In general, Fig. 9 shows that increasing M makes the development length shorter. On the contrary, Figs. 5, 7, and 8 show that increasing M moves the predicted central plug farther into the pipe or channel, and makes the stress evolution just upstream of it more gradual. Thus higher values of M predict a faster initial flow development near the inlet, possibly due to higher stresses, followed by a slower development afterwards, compared to lower values of M .

Let us now examine what Fig. 9 tells us about the flow. A salient feature of all diagrams is that they exhibit a sharp minimum, at about $\tilde{r} \approx 0.6 - 0.65$ or $\tilde{y} \approx 0.55 - 0.6$, which can be explained thus: Since the flow, initially uniform at the inlet, decelerates near the walls and accelerates near the centre, there must be some intermediate point where the fully developed velocity is equal to that at the inlet. It is there that the development length is minimal – albeit not zero, because the velocity, even there, undergoes some fluctuation before resettling to the same value that it had at the inlet. This point separates the accelerating from the decelerating region, both of which have local L maxima. The maximum of the decelerating region occurs exactly at the wall, and is a bit larger than that of the accelerating region, although not by a wide margin – especially in the axisymmetric case they are nearly equal.

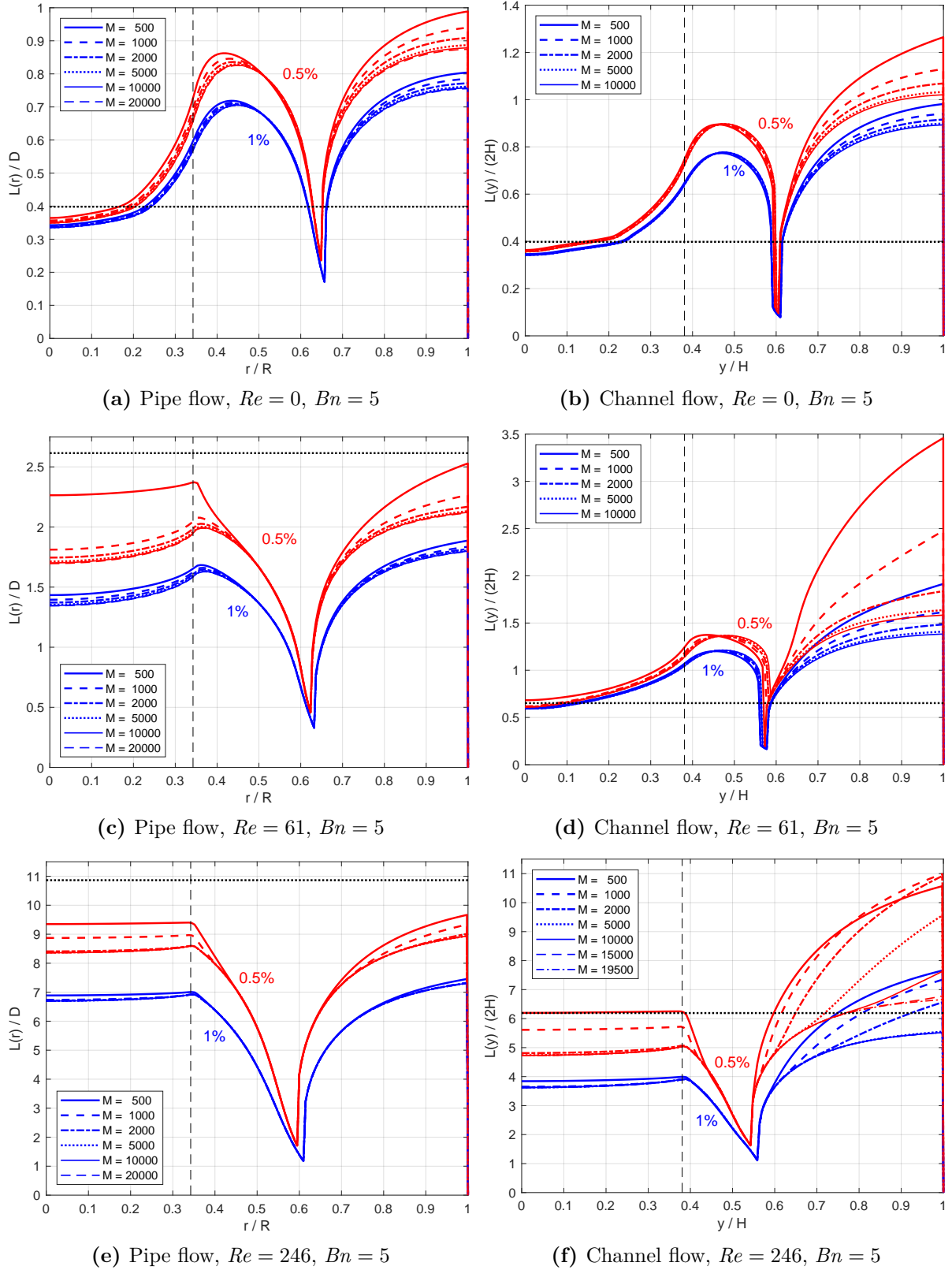


Figure 9: Variation of the development length $L(r)$ or $L(y)$ across the pipe radius (left column) or channel width (right column), for $Bn = 5$ and $Re = 0$ (top row), $Re = 61$ (middle row), and $Re = 246$ (bottom row). Results obtained with different values of M are compared. Blue and red lines denote the development lengths based on 1% and 0.5% margins from the fully developed velocity, respectively. The black vertical dashed line marks the fully developed plug radius (calculated analytically). The black horizontal dotted line marks the tip of the plug (obtained from the $M = 10000$ results).

In the creeping-flow axisymmetric case (Fig. 9a), the local maximum of L in the accelerating region occurs at about $\tilde{r} \approx 0.43$, which is beyond the fully developed plug radius $\tilde{r}_0 \approx 0.34$ (see Table 1 and the vertical dashed line in Fig. 9a). At the centre of the pipe ($\tilde{r} = 0$) the development length is slightly shorter (by about $0.05D$) than the distance where the tip of the core plug forms (marked with a horizontal dotted line in the figure). Interestingly, from $\tilde{r} \approx 0.2$ up to the fully developed core plug radius $\tilde{r}_0 \approx 0.34$, the development length (either $L_{1\%}$ or $L_{0.5\%}$) extends deeper inside the pipe than the tip of the core plug. This, of course, does not mean that flow development is completed inside the plug, something that is impossible since the velocity inside the core plug is everywhere fully-developed and constant. Rather, because the upstream edge of the core plug is not flat but tapered, as seen in Fig. 3, at these radii the flow becomes developed somewhere past the tip of the core plug but inside yielded material nonetheless. Very similar observations can be made about the planar case, Fig. 9b.

As the Reynolds number is increased (Figs. 9c, 9e) the local maximum of the accelerating region moves towards r_0 , while the $L(r)$ distribution for $0 \leq r \leq r_0$ becomes flat; thus, the cylindrical volume of yielded fluid of radius r_0 that extends some distance upstream from the central plug also exhibits some plug-like characteristics. Both the 1% and the 0.5% developments occur prior to the formation of the central plug. Similar observations hold also for the planar case (Figs. 9d, 9f).

Figures 10 and 11 compare the three main development lengths, L_c , L_g and $L_{\tau w}$, for axisymmetric and planar flow, respectively. To obtain the data, simulations were performed where the Bingham number was held fixed and the Reynolds number was varied, and the three development lengths were recorded. The procedure was repeated for a set of different Bingham numbers, listed in Table 1 along with the corresponding plug radii/thicknesses.

In accordance with previous studies, the diagrams show that the development length tends to a finite (Bn -dependent) value as $Re \rightarrow 0$; it exhibits an approximately constant plateau at low Re values and increases proportionally to Re at higher Re values. This holds for all development lengths, including the newly-proposed $L_{\tau w}$. In Newtonian flow, L_c and

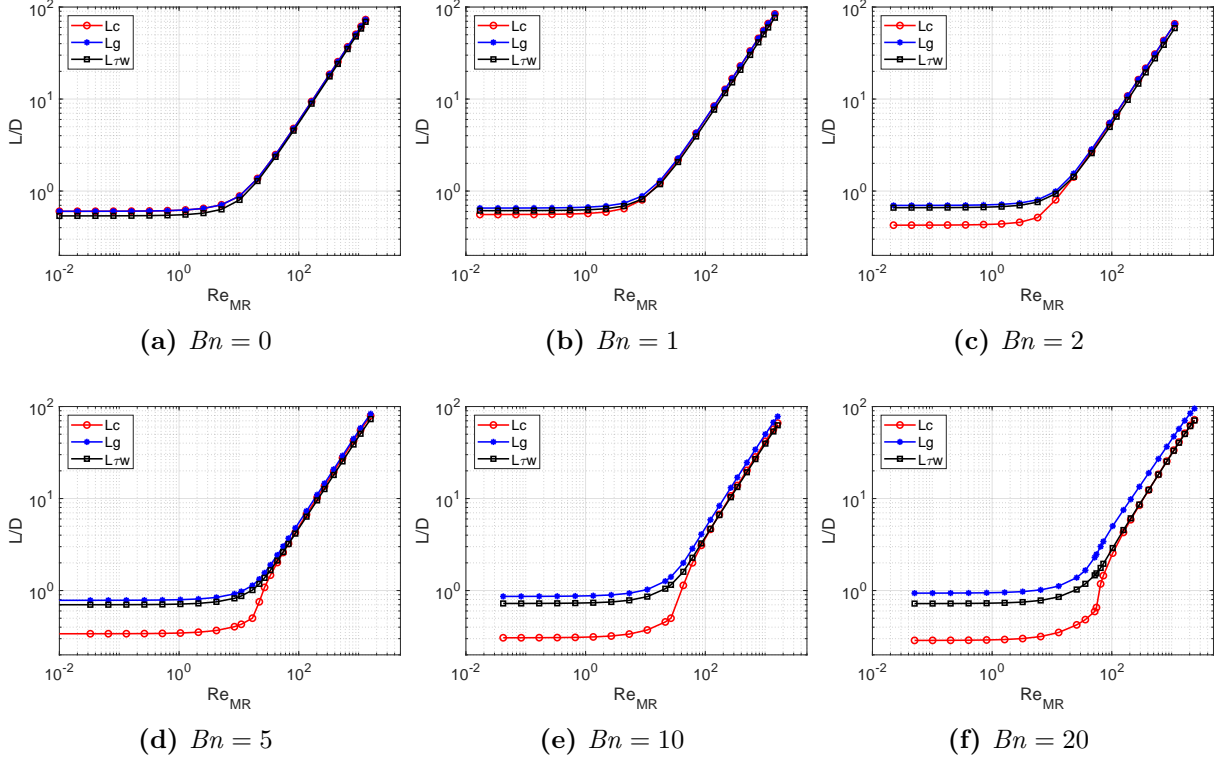


Figure 10: Pipe flow: Comparison of the variations of the three development lengths with the Reynolds number for different Bingham numbers. For convenience, the Metzner-Reed Reynolds number (Eq. (27)) is used instead of Re so as to use the same x -axis range for all plots. Computed with $M = 2000$.

L_g are identical and L_{τ_w} is very slightly smaller. As the Bingham number is increased, the value of L_c in the low- Re plateau decreases because the central plug expands and its flat velocity tends to equate to that at the inlet, so that less development is required near the centre [13, 10]. However, the other two development lengths, L_g and L_{τ_w} , actually increase with Bn : the rapid development at the central region due to the expansion of the plug is balanced by a slower flow development near the walls. Although at low Re increase of Bn causes divergence between L_c on one hand and L_g and L_{τ_w} on the other, beyond some value of Re the length L_c catches up rapidly with the other lengths – or at least with L_{τ_w} , because L_g starts to pull away from the rest at high Bn . More insight is provided by Fig. 9 (where, for $Bn = 5$, $Re = 61$ translates to $Re_{MR} = 33/28$ for pipe/channel flow, and $Re = 246$ translates to $Re_{MR} = 135/112$, respectively), which shows that at higher Reynolds numbers L_c is quite close to the maximum value of $L(r)$ in the accelerating region, while $L(r)$ attains even higher values (albeit not much higher) in the decelerating region, and in particular at the wall: $L_g = L(R)$. The same hold also for the planar case.

The accurate calculation of L_g for high- Bn planar flow is quite challenging, due to

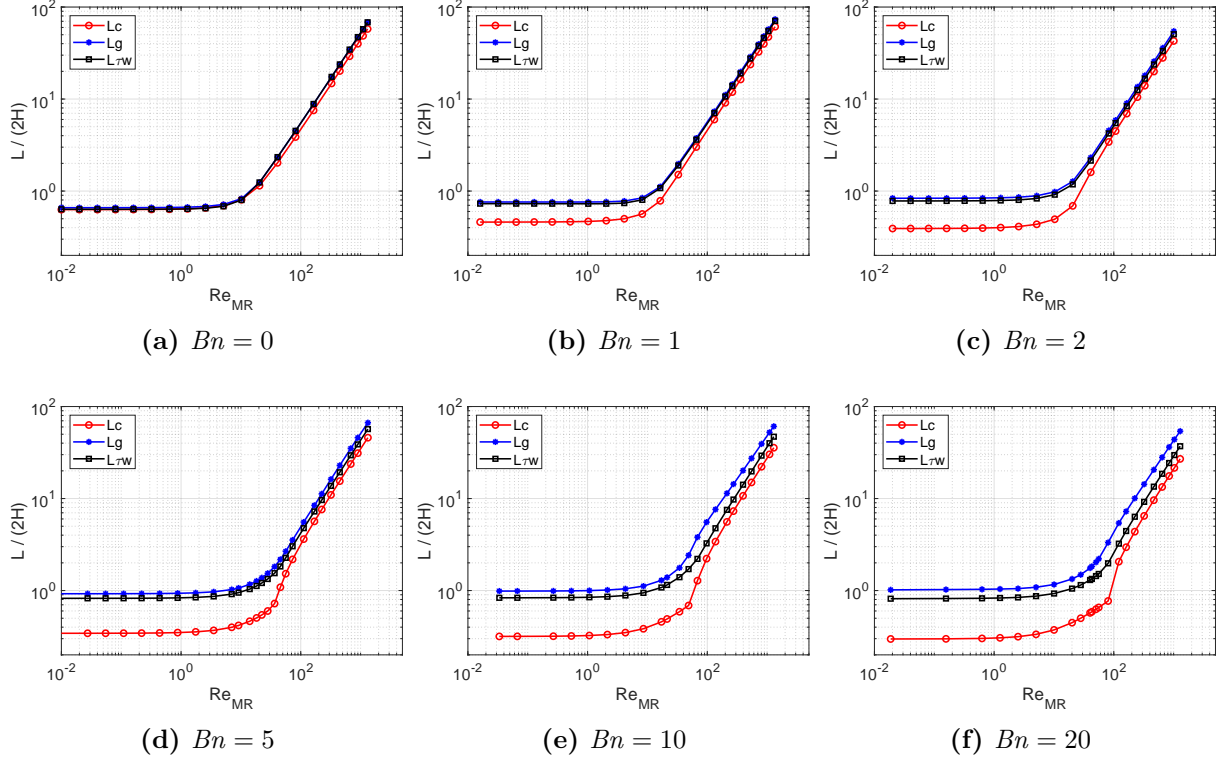


Figure 11: Channel flow: Comparison of the variations of the three development lengths with the Reynolds number for different Bingham numbers. For convenience, the Metzner-Reed Reynolds number (Eq. (28)) is used instead of Re so as to use the same x -axis range for all plots. The computations were performed with $M = 2000$ (for $Bn = 1$ and 2), $M = 5000$ (for $Bn = 5$ and 10) and $M = 15000$ (for $Bn = 20$).

a tendency to exaggerate the development length close to the wall, exhibited in Fig. 9f. Figure 12a compares the results obtained with different values of M . This exaggeration is manifested as a spurious “hump” exhibited by the L_g curves in the approximate range $25 \leq Re_{MR} \leq 500$, which decreases as M is increased. Interestingly, the difficulty appears to vanish not only at small Reynolds numbers but also at large ones ($Re_{MR} > 500$), for which even $M = 2000$ seems to provide good accuracy. Figure 12b shows the corresponding variations of $L_{\tau w}$, for which the errors appear to be much smaller – the results for $M = 5000$ and $M = 15000$ are almost indistinguishable. This is a fortunate and perhaps surprising observation given that $L_{\tau w}$ is also determined by the flow conditions at the wall.

The x -axis of Figs. 10 and 11 is in terms of the Metzner-Reed Reynolds number, which facilitates using the same x -axis ranges in all plots, irrespective of the Bingham number. This brings us to the issue of examining the various Reynolds number variants of Sec. 3 and how the development lengths correlate to them. The results are plotted in Figs.

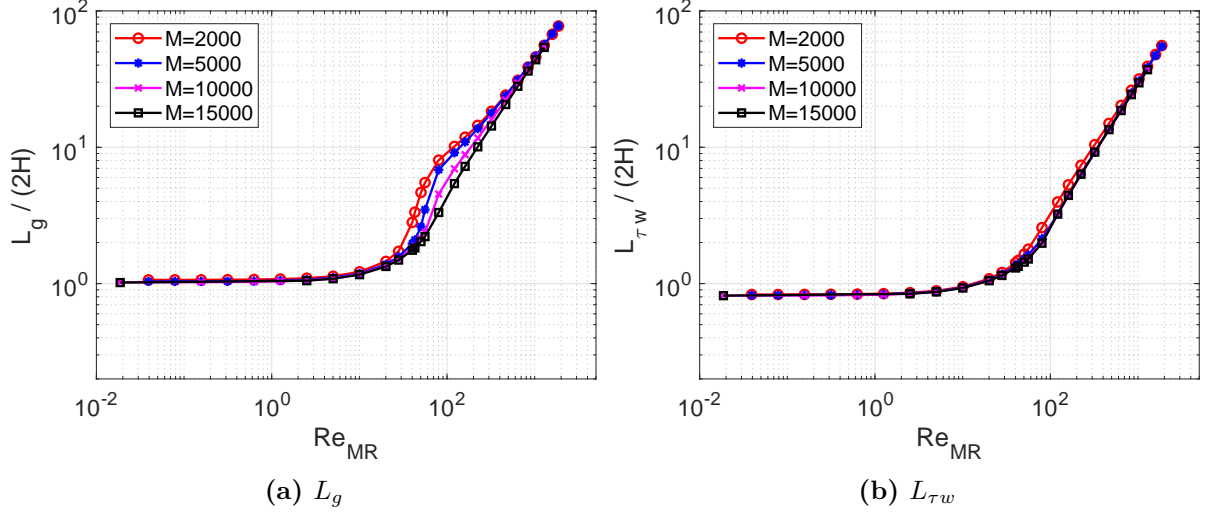


Figure 12: Variations of L_g (a) and L_{τ_w} (b) with Re_{MR} for the $Bn = 20$ planar case, obtained with various values of M .

13-16.

It is no surprise that when the development lengths are plotted against the standard Reynolds number Re (7) then the curves for the various Bingham numbers are spaced apart (Figs. 13a-13c for axisymmetric flow, 15a-15c for planar flow); as the Bingham number is increased, the same trends are observed as for lower Bn but delayed to higher Re . At low Re , the L_c 's are more dispersed for the various Bn compared to L_g and L_{τ_w} .

The “effective” Reynolds numbers, Re^{*D} and Re^{*R} (or Re^{*2H} and Re^{*H}) go some way towards bringing the different Bn curves together. In Figs. 13d, 13e and 13f we can see that the higher the Bingham number the more shifted the curves are towards the left, which suggests that the characteristic stress inherent in Re^{*D} , $\tau_0 + \mu U/D$, grows faster with Bn than the actual characteristic stress that determines the development length. Re^{*R} , which uses the characteristic stress $\frac{1}{2}(\tau_0 + \mu U/R)$ does a better job, as seen in Figs. 13g, 13h and 13i; the shifting of the curves towards the left with increase of Bn is still exhibited, but to a smaller degree. The planar case (Figs. 15d–15i) is similar, and in fact the correlations are better than in the axisymmetric case. Especially Re^{*H} (Figs. 15g–15i) is quite effective in collapsing the development length curves for all Bn .

Let us now turn to Reynolds numbers that employ the wall shear stress as a characteristic stress. Figures 13j–13l plot the development lengths with respect to Re_{MR} , for pipe flow. What is immediately striking is the near-perfect collapse of the L_g curves (Fig.

13k). On the other hand, L_c and $L_{\tau w}$ seem somewhat more dispersed than when plotted against Re^{*R} . In fact the L_c and $L_{\tau w}$ curves are now displaced towards the right as Bn is increased, which means that Re_{MR} overestimates the ratio of inertia to viscoplastic resistance that is determining these development lengths. If then we apply a correction to the momentum flux in the numerator as in Re_{MRC} , then we observe a slight improvement in Figs. 14a–14c. The $L_g(Re_{MRC})$ correlations are almost perfectly matched, while the $L_c(Re_{MRC})$ and $L_{\tau w}(Re_{MRC})$ curves are slightly closer together compared to $L_c(Re_{MR})$ and $L_{\tau w}(Re_{MR})$ but some noticeable dispersion persists. Interestingly, the Reynolds number of Ookawara et al., Re_O , (Figs. 14d–14f) does a markedly better job collapsing the L_c and $L_{\tau w}$ curves, albeit at the expense of the L_g curves. Similar observations hold true also for the planar case (Figs. 16a–16f).

Finally, we consider the remaining Reynolds numbers, which account only for the increase in the momentum or energy of the fluid rather than the total amount. As seen in Fig. 14g, Re_{MG} is the most effective Reynolds number for collapsing the L_c curves. This is not surprising given that the the flow development dynamics near the axis is governed to a large extent by the fact that higher viscoplasticity (Bingham number) brings the fully developed plug velocity closer to the inlet velocity thereby reducing the required development length. Consequently, near the pipe centre the change in momentum between the inlet and the fully developed state is more relevant to the determination of the development length than the fully developed momentum as a whole. However, this is not the case close to the walls, which explains why Re_{MG} performs less effectively regarding L_g (Fig. 14h); nevertheless, the $L_g(Re_{MG})$ correlation is quite decent, surpassed only by $L_g(Re_{MR})$ and $L_g(Re_{MRC})$. On the other hand, perhaps surprisingly, Re_{MG} is also the most effective Reynolds number for collapsing the $L_{\tau w}$ curves, despite $L_{\tau w}$ referring to conditions at the wall. In fact, returning to Fig. 10, we notice that while in the creeping flow regime L_c and $L_{\tau w}$ differ substantially, in the inertia-dominated regime they converge onto a single curve, for all values of Bn considered, while L_g is larger. So, once inertia begins to become prominent, the development of the core flow determines also the development of the wall shear stress ($L_{\tau w} = L_c$); while the flow near the walls continues

to develop for a larger distance ($L_g > L_{\tau_w}$), this development seems to occur in a way that does not impact the wall shear stress. As for the last Reynolds number, Re_{EG} , a comparison between Figs. 14j–14l and Figs. 14g–14i shows that it exhibits the same traits as Re_{MG} , but it is slightly less effective than the latter.

Turning to the channel flow case, we can make similar observations although the $L_{\tau_w}(Re_{MG})$ and especially the $L_g(Re_{MG})$ correlations are not as good as in the pipe flow case. Now in Fig. 11 one can see that L_c and L_{τ_w} do not coincide even in the region of prominent inertia, with L_{τ_w} being consistently greater. Therefore the equality of L_c and L_{τ_w} is particular to the pipe flow case and cannot be generalised to all conduit geometries.

The last set of results to be discussed here concern the variation of the development lengths with the Bingham number, plotted in Fig. 17. The focus is on the inertialess case (Figs. 17a and 17b) because when inertia is important then the development length is determined by an appropriate effective Reynolds number, and not by the Bingham number per se. In that case, increasing the Bingham number is equivalent to lowering the effective Reynolds number, thus causing a reduction of the development lengths as studied extensively in the previous discussion of the correlation of the lengths with the several Reynolds number variants. An indicative plot is Fig. 17c where the standard Reynolds number is held at $Re = 246$ and the reduction of all development lengths as the Bingham number is increased (and the effective Reynolds numbers are therefore decreased) is apparent. But in the low inertia regime the Reynolds number becomes irrelevant and the development lengths are determined by the Bingham number alone. The behaviour of the development length in this regime is summarised in Figs. 17a and 17b for pipe and channel flow, respectively. In both cases, L_c decreases and L_g increases with Bn , as already noted in [13]. The new piece of data in Figs. 17a and 17b is the variation of L_{τ_w} which, interestingly, is non-monotonic. Up to a Bingham number of about 10, L_{τ_w} increases with Bn , similarly to L_g , but thereafter it decreases, similarly to L_c (and in fact at a faster rate). Due to this non-monotonous behaviour, L_{τ_w} varies less in the range considered ($0 \leq Bn \leq 50$) compared to L_g and L_c : $L_{\tau_w} \in (0.57, 0.72)$ in the axisymmetric case, and $L_{\tau_w} \in (0.70, 0.83)$ in the planar case.

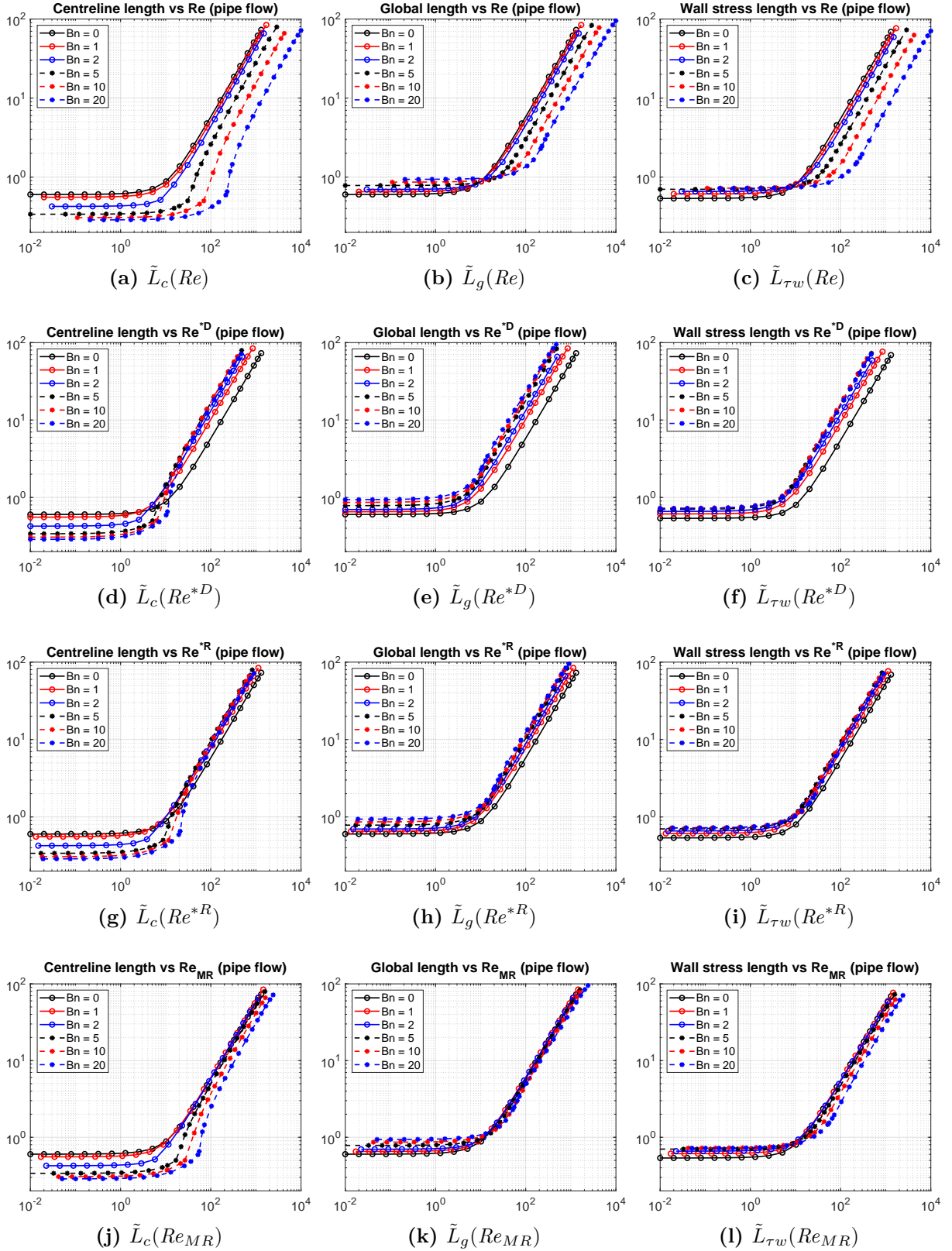


Figure 13: Pipe flow at various Bingham numbers: The three development lengths L_c (left), L_c (middle) and L_{τ_w} (right), scaled by the pipe diameter D , as a function of Re (7) (top row), Re^{*D} (23) (2nd row), Re^{*R} (24) (3rd row), and Re_{MR} (27) (last row).

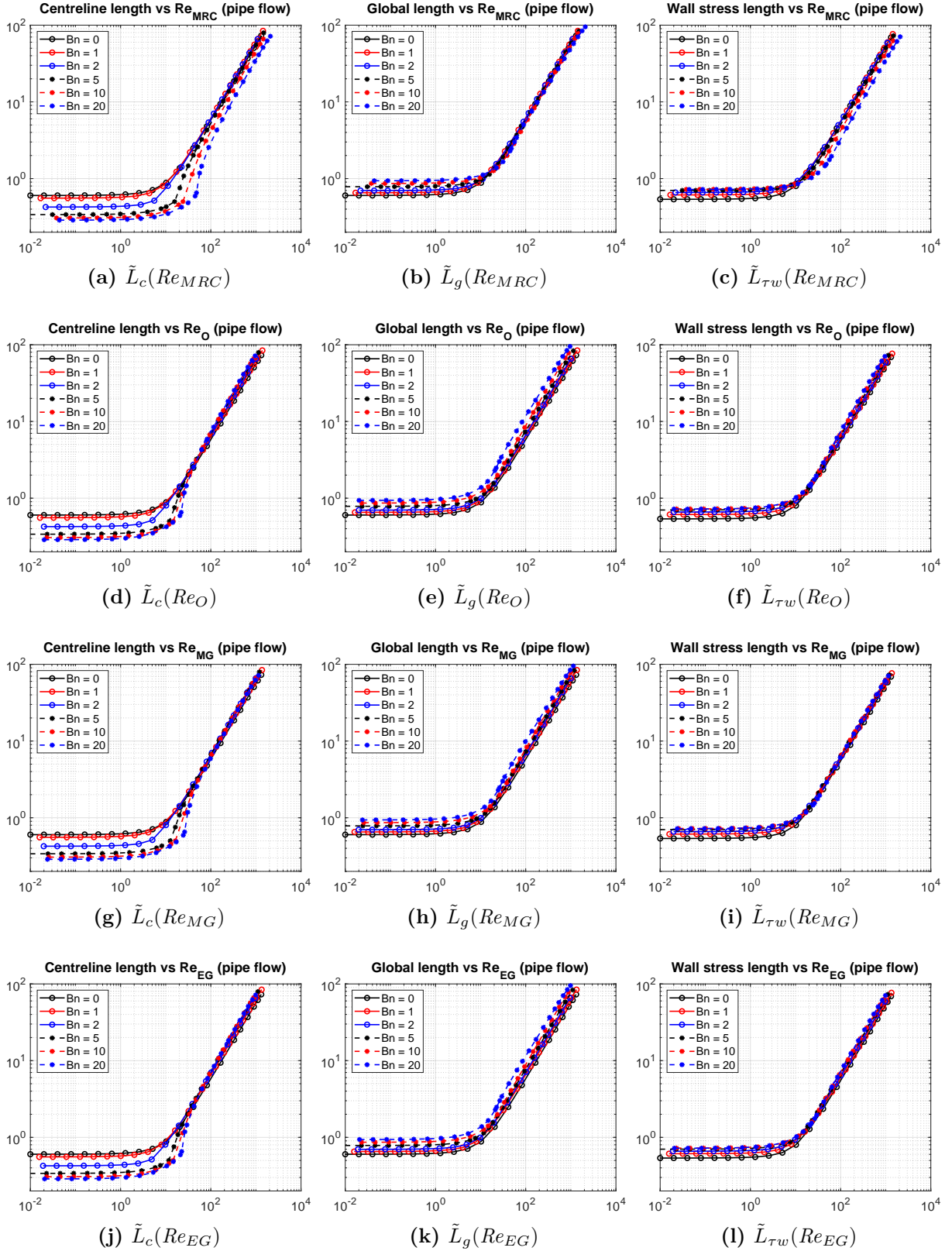


Figure 14: Pipe flow at various Bingham numbers: The three development lengths L_c (left), L_c (middle) and L_{τ_w} (right), scaled by the pipe diameter D , as a function of Re_{MRC} (30) (top row), Ookawara's Reynolds number [7] (2nd row, denoted as Re_O), Re_{MG} (37) (3rd row), and Re_{EG} (41) (last row).

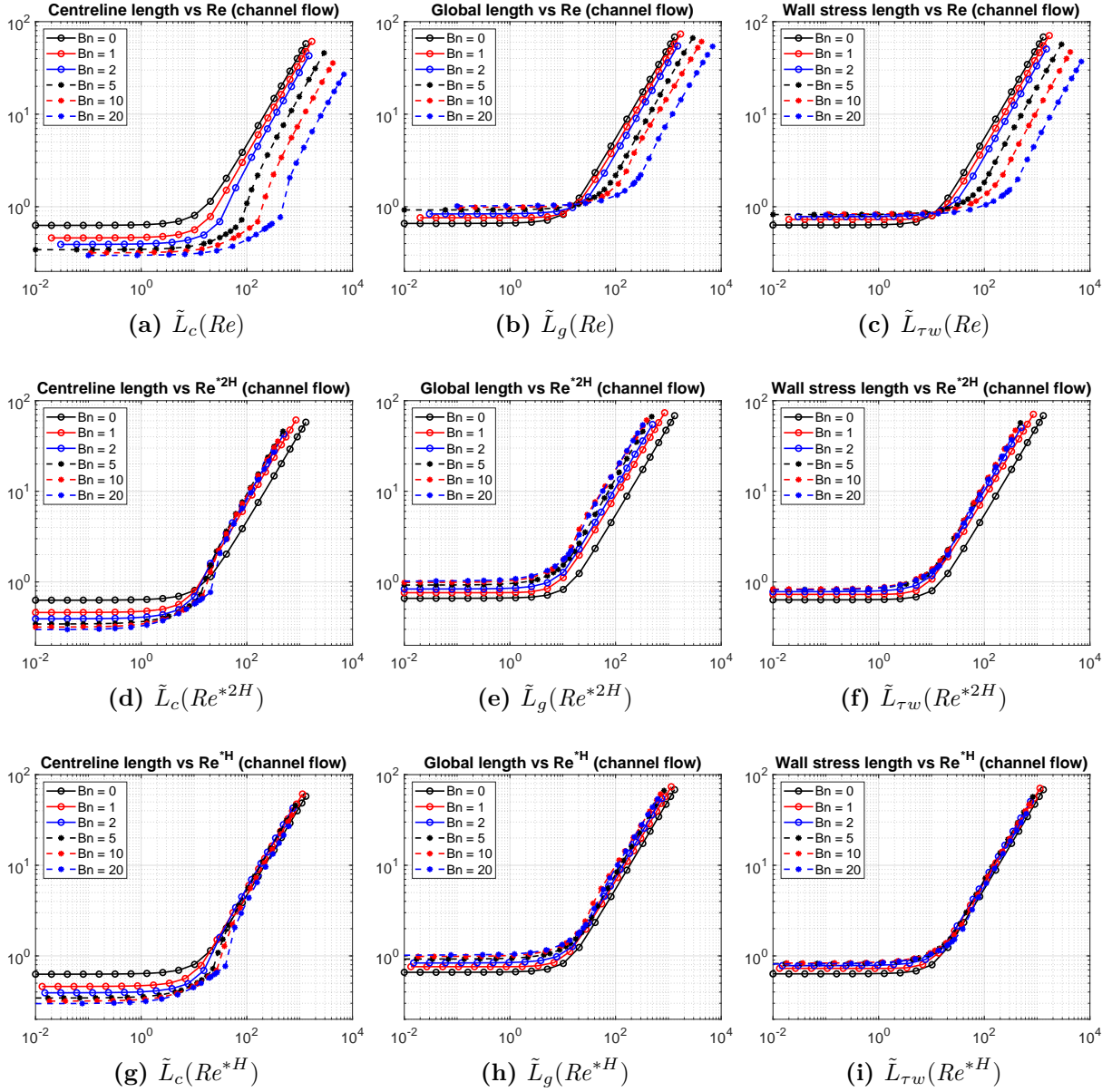


Figure 15: Channel flow at various Bingham numbers: The three development lengths L_c (left), L_c (middle) and L_{τ_w} (right), scaled by the channel height diameter $2H$, as a function of Re (top row), Re^{*2H} (2nd row), and Re^{*H} (last row).

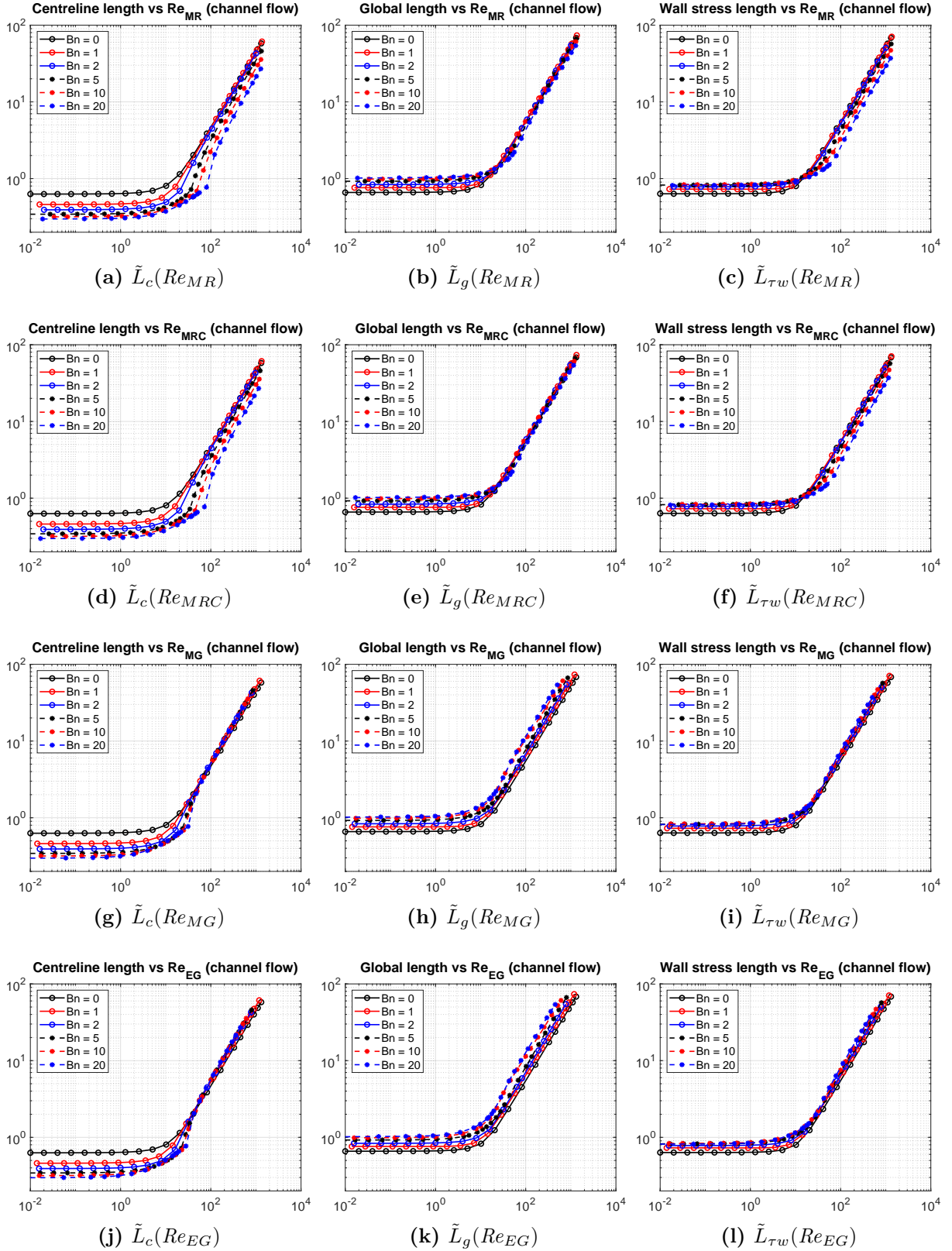
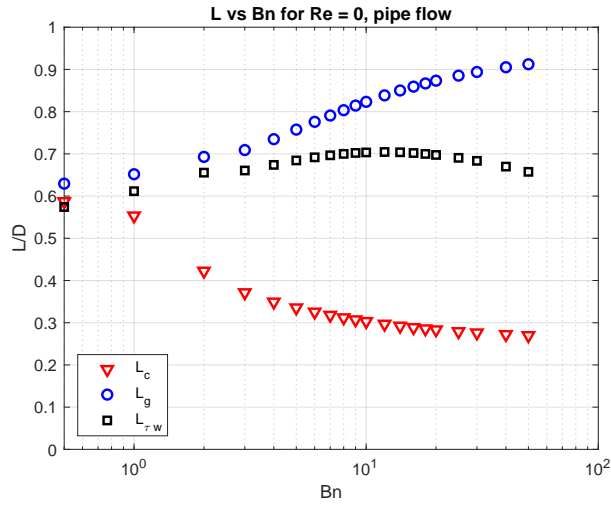
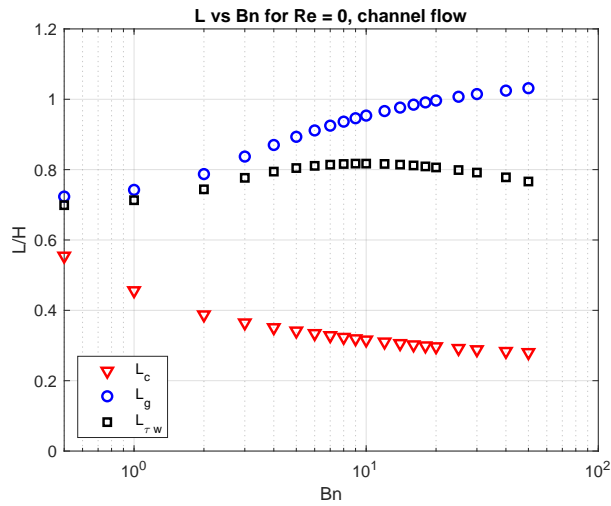


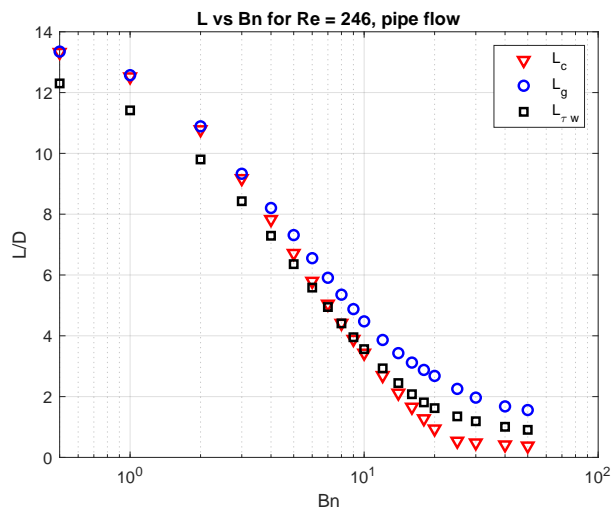
Figure 16: Channel flow at various Bingham numbers: The three development lengths L_c (left), L_g (middle) and L_{τ_w} (right), scaled by the channel height diameter $2H$, as a function of Re_{MR} (top row), Re_{MRC} (2nd row), Re_{MG} (3rd row), and Re_{EG} (last row).



(a)



(b)



(c)

Figure 17: Variation of the development lengths with the Bingham number: (a) creeping ($Re = 0$) pipe flow with $M = 10000$; (b) creeping ($Re = 0$) channel flow with $M = 10000$; (c) pipe flow at $Re = 246$ with $M = 2000$.

5. Conclusions

We have revisited the problem of laminar flow development of viscoplastic fluids by means of finite element simulations, employing the Papanastasiou regularisation of the Bingham plastic equation. We have focused on three definitions of the development length, based on the centreline velocity (L_c), the global velocity field (L_g), and the wall shear stress ($L_{\tau w}$). Usually, it was found that $L_c < L_{\tau w} < L_g$, although at very low Bingham numbers L_c and L_g are identical or nearly identical and $L_{\tau w}$ is slightly smaller than them.

In an effort to collapse the development length versus Reynolds number curves onto a single master curve, we tested several alternative definitions of the Reynolds number. The results showed that the “momentum gain” Reynolds number, Re_{MG} , (Eq. (36)) is most effective in accomplishing this for L_c and $L_{\tau w}$, both for pipe and channel flow, while for L_g the most effective choice is Re_{MRC} , the corrected “Metzner-Reed” Reynolds number (Eq. (29)). The uncorrected “Metzner-Reed” Reynolds number (Eq. (26)) is almost as effective, and does not require knowledge of the fully-developed velocity profile (it requires knowledge of the wall shear stress, but in an experimental setting this is easy to obtain from the pressure gradient). An even simpler choice is the effective Reynolds number based on the pipe diameter or channel half-width, Re^{*R} or Re^{*H} , (Eq. (24)) which is not as effective but still has a decent performance.

In the low-inertia regime the development length curves are impossible to collapse as they are independent of the Reynolds number and depend only on the Bingham number. In this regime, L_c decreases with the Bingham number, L_g exhibits the opposite behaviour, while $L_{\tau w}$ is non-monotonic, increasing with Bn up to a value of $Bn \approx 10$ and decreasing thereafter.

Near the entrance, there are three unyielded regions in planar flow, one of which develops downstream into the fully developed unyielded core plug. In axisymmetric flow, one of these regions is absent due to physical constraints. As the Reynolds number is increased, the formation of the core plug is pushed farther into the pipe or channel, and the flow development is more gradual, necessitating higher values of the regularisation parameter to maintain accuracy.

It will be interesting to extend the current study to cases with shear-thinning (or thickening), by employing the Herschel-Bulkley model, and to cases with wall slip, both of which are common in actual viscoplastic flows. Such a study may be undertaken in the near future.

Acknowledgements

This study was funded by the Cohesion Policy Programme “THALIA 2021-2027”, co-funded by the European Union, through the Research and Innovation Foundation of Cyprus (Project “CRaFTC” – SMALL SCALE INFRASTRUCTURES/1222/0181).

References

- [1] A. S. Haase, J. A. Wood, L. M. J. Sprakel, and R. G. H. Lammertink, “Inelastic non-Newtonian flow over heterogeneously slippery surfaces,” *Physical Review E*, vol. 95, no. 2, p. 023105, 2017.
- [2] D. Pasiadis, A. Passos, G. Constantinides, S. Balabani, and E. Kaliviotis, “Surface tension driven flow of blood in a rectangular microfluidic channel: Effect of erythrocyte aggregation,” *Physics of Fluids*, vol. 32, no. 7, p. 071903, 2020.
- [3] J. B. Grotberg, *Biofluid Mechanics: Analysis and Applications*. Cambridge University Press, 2021.
- [4] A. R. Clark, M. Lin, M. Tawhai, R. Saghian, and J. L. James, “Multiscale modelling of the feto-placental vasculature,” *Interface Focus*, vol. 5, no. 2, p. 20140078, 2015.
- [5] S. L. Kfuri, J. Q. Silva, E. J. Soares, and R. L. Thompson, “Friction losses for power-law and viscoplastic materials in an entrance of a tube and an abrupt contraction,” *Journal of Petroleum Science and Engineering*, vol. 76, no. 3–4, pp. 224–235, 2011.
- [6] F. Durst, S. Ray, B. Ünsal, and O. A. Bayoumi, “The development lengths of laminar pipe and channel flows,” *Journal of Fluids Engineering*, vol. 127, no. 6, pp. 1154–1160, 2005.

- [7] S. Ookawara, K. Ogawa, N. Dombrowski, E. Amooie-Foumeny, and A. Riza, “Unified entry length correlation for Newtonian, power law and Bingham fluids in laminar pipe flow at low Reynolds number.,” *Journal of Chemical Engineering of Japan*, vol. 33, no. 4, pp. 675–678, 2000.
- [8] R. J. Poole and B. S. Ridley, “Development-length requirements for fully developed laminar pipe flow of inelastic non-Newtonian liquids,” *Journal of Fluids Engineering*, vol. 129, no. 10, pp. 1281–1287, 2007.
- [9] C. Fernandes, L. Ferrás, M. Araujo, and J. Nóbrega, “Development length in planar channel flows of inelastic non-Newtonian fluids,” *Journal of Non-Newtonian Fluid Mechanics*, vol. 255, pp. 13–18, 2018.
- [10] C. Lambride, A. Syrakos, and G. C. Georgiou, “Entrance length estimates for flows of power-law fluids in pipes and channels,” *Journal of Non-Newtonian Fluid Mechanics*, vol. 317, p. 105056, 2023.
- [11] R. J. Soto and V. L. Shah, “Entrance flow of a yield-power law fluid,” *Applied Scientific Research*, vol. 32, no. 1, pp. 73–85, 1976.
- [12] R. J. Poole and R. P. Chhabra, “Development length requirements for fully developed laminar pipe flow of yield stress fluids,” *Journal of Fluids Engineering*, vol. 132, no. 3, p. 034501, 2010.
- [13] M. Philippou, Z. Kountouriotis, and G. C. Georgiou, “Viscoplastic flow development in tubes and channels with wall slip,” *Journal of Non-Newtonian Fluid Mechanics*, vol. 234, pp. 69–81, 2016.
- [14] P. Panaseti and G. C. Georgiou, “Viscoplastic flow development in a channel with slip along one wall,” *Journal of Non-Newtonian Fluid Mechanics*, vol. 248, pp. 8–22, 2017.
- [15] K. Yapici, B. Karasozen, and Y. Uludag, “Numerical analysis of viscoelastic fluids in steady pressure-driven channel flow,” *Journal of Fluids Engineering*, vol. 134, no. 5, p. 051206, 2012.

- [16] J. Bertoco, R. T. Leiva, L. L. Ferrás, A. M. Afonso, and A. Castelo, “Development length of fluids modelled by the gPTT constitutive differential equation,” *Applied Sciences*, vol. 11, no. 21, p. 10352, 2021.
- [17] Z. Kountouriotis, M. Philippou, and G. C. Georgiou, “Development lengths in Newtonian Poiseuille flows with wall slip,” *Applied Mathematics and Computation*, vol. 291, pp. 98–114, 2016.
- [18] M. Zhou, Y. Yu, R. Chen, X. Liu, Y. Hu, Z. Ma, L. Gao, W. Jian, and L. Wang, “Wall shear stress and its role in atherosclerosis,” *Frontiers in Cardiovascular Medicine*, vol. 10, p. 1083547, 2023.
- [19] A. B. Metzner and J. C. Reed, “Flow of non-Newtonian fluids—correlation of the laminar, transition, and turbulent-flow regions,” *AIChE Journal*, vol. 1, no. 4, pp. 434–440, 1955.
- [20] M. S. Oliveira, P. J. Oliveira, F. T. Pinho, and M. A. Alves, “Effect of contraction ratio upon viscoelastic flow in contractions: The axisymmetric case,” *Journal of Non-Newtonian Fluid Mechanics*, vol. 147, no. 1–2, pp. 92–108, 2007.
- [21] Z. Li and S. J. Haward, “Viscoelastic flow development in planar microchannels,” *Microfluidics and Nanofluidics*, vol. 19, no. 5, pp. 1123–1137, 2015.
- [22] A. Syrakos, Y. Dimakopoulos, and J. Tsamopoulos, “Theoretical study of the flow in a fluid damper containing high viscosity silicone oil: Effects of shear-thinning and viscoelasticity,” *Physics of Fluids*, vol. 30, no. 3, p. 030708, 2018.
- [23] P. Corvisier, C. Nouar, R. Devienne, and M. Lebouché, “Development of a thixotropic fluid flow in a pipe,” *Experiments in Fluids*, vol. 31, no. 5, pp. 579–587, 2001.
- [24] L. Zhang, H. Wang, A. Wu, K. Yang, and P. Kong, “Simulation of circular pipe flow of thixotropic cemented tailings pastes,” *Chemical Engineering Research and Design*, vol. 196, pp. 671–684, 2023.

- [25] T. C. Papanastasiou, “Flows of materials with yield,” *Journal of Rheology*, vol. 31, no. 5, pp. 385–404, 1987.
- [26] E. Mitsoulis, “Flows of viscoplastic materials: models and computations,” *Rheology Reviews*, pp. 135–178, 2007.
- [27] A. Syrakos, G. C. Georgiou, and A. N. Alexandrou, “Solution of the square lid-driven cavity flow of a Bingham plastic using the finite volume method,” *Journal of Non-Newtonian Fluid Mechanics*, vol. 195, pp. 19–31, 2013.
- [28] A. Syrakos, G. C. Georgiou, and A. N. Alexandrou, “Performance of the finite volume method in solving regularised Bingham flows: Inertia effects in the lid-driven cavity flow,” *Journal of Non-Newtonian Fluid Mechanics*, vol. 208–209, pp. 88–107, 2014.
- [29] M. Alnæs, J. Blechta, J. Hake, A. Johansson, B. Kehlet, A. Logg, C. Richardson, J. Ring, M. E. Rognes, and G. N. Wells, “The FEniCS project version 1.5,” *Archive of Numerical Software*, vol. 3, 2015.
- [30] N. Nirmalkar, R. Chhabra, and R. Poole, “Laminar forced convection heat transfer from a heated square cylinder in a bingham plastic fluid,” *International Journal of Heat and Mass Transfer*, vol. 56, no. 1–2, pp. 625–639, 2013.
- [31] A. Syrakos, G. C. Georgiou, and A. N. Alexandrou, “Cessation of the lid-driven cavity flow of newtonian and bingham fluids,” *Rheologica Acta*, vol. 55, no. 1, pp. 51–66, 2016.
- [32] R. L. Thompson and E. J. Soares, “Viscoplastic dimensionless numbers,” *Journal of Non-Newtonian Fluid Mechanics*, vol. 238, pp. 57–64, 2016.
- [33] M. A. Ferrari and A. T. Franco, “The steady and unsteady regimes in a cubic lid-driven cavity with viscoplastic fluid solved with the lattice Boltzmann method,” *Journal of Non-Newtonian Fluid Mechanics*, vol. 325, p. 105198, 2024.
- [34] Y. Dimakopoulos, G. Makrigiorgos, G. Georgiou, and J. Tsamopoulos, “The PAL (Penalized Augmented Lagrangian) method for computing viscoplastic flows: A

- new fast converging scheme,” *Journal of Non-Newtonian Fluid Mechanics*, vol. 256, pp. 23–41, 2018.
- [35] S. Varchanis, S. J. Haward, C. C. Hopkins, A. Syrakos, A. Q. Shen, Y. Dimakopoulos, and J. Tsamopoulos, “Transition between solid and liquid state of yield-stress fluids under purely extensional deformations,” *Proceedings of the National Academy of Sciences*, vol. 117, no. 23, pp. 12611–12617, 2020.
- [36] A. Syrakos, G. C. Georgiou, and A. N. Alexandrou, “Thixotropic flow past a cylinder,” *Journal of Non-Newtonian Fluid Mechanics*, vol. 220, pp. 44–56, 2015.
- [37] Y. Dimakopoulos, M. Pavlidis, and J. Tsamopoulos, “Steady bubble rise in Herschel–Bulkley fluids and comparison of predictions via the augmented Lagrangian method with those via the Papanastasiou model,” *Journal of Non-Newtonian Fluid Mechanics*, vol. 200, pp. 34–51, 2013.